The Intensification of Two-Dimensional Swirling Flows by Stochastic Asymmetric Forcing

DAVID S. NOLAN*

Department of Mathematics, Lawrence Berkeley National Laboratory, Berkeley, California

BRIAN F. FARRELL

Department of Earth and Planetary Sciences, Harvard University, Cambridge, Massachusetts

(Manuscript received 29 October 1997, in final form 24 December 1998)

ABSTRACT

The effects of stochastically excited asymmetric disturbances on two-dimensional vortices are investigated. These vortices are maintained by the radial inflow of fixed cylindrical deformation fields, which are chosen so that both one-celled and two-celled vortices may be studied. The linearized perturbation equations are reduced to the form of a linear dynamical system with stochastic forcing, that is, $d\mathbf{x}/dt = \mathbf{A}\mathbf{x} + \mathbf{F}\boldsymbol{\xi}$, where the columns of $\mathbf{F}$ are forcing functions and the elements of $\boldsymbol{\xi}$ are Gaussian white-noise processes. Through this formulation the stochastically maintained variance of the perturbations, the structures that dominate the response (the empirical orthogonal functions), and the forcing functions that contribute most to this response (the stochastic optimals) can be directly calculated.

For all cases the structures that most effectively induce the transfer of energy from the mean flow to the perturbation field are close approximations to the global optimals (i.e., the initial perturbations with the maximum growth in energy in finite time), and that the structures that account for most of the variance are close approximations to the global optimals evolved forward in time to when they reach their maximum energy. For azimuthal wavenumbers in each vortex where nearly neutral modes are present ($k = 1$ for the one-celled vortex and $1 \leq k \leq 4$ for the two-celled vortex), the variance sustained by the stochastic forcing is large, and in these cases the variance may be greatly overestimated if the radial inflow that sustains the mean vortex is neglected in the dynamics of the perturbations.

Through a modification of this technique the ensemble average eddy momentum flux divergences associated with the stochastically maintained perturbation fields can be computed, and this information is used to determine the perturbation-induced mean flow tendency in the linear limit. Examination of these results shows that the net effect of the low wavenumber perturbations is to cause downgradient eddy fluxes in both vortex types, while high wavenumber perturbations cause upgradient eddy fluxes. However, to determine how these eddy fluxes actually change the mean flow, the local accelerations caused by the eddy flux divergences must be incorporated into the equation for the steady-state azimuthal velocity. From calculations of this type, it is found that the effect of the radial inflow can be crucial in determining whether or not the vortex is intensified or weakened by the perturbations: though the net eddy fluxes are most often downgradient, the radial inflow carries the transported angular momentum back into the vortex core, resulting in an increase in the maximum wind speed. In most cases for the vortex flows studied, the net effect of stochastically forced asymmetric perturbations is to intensify the mean vortex. Applications of the same analysis techniques to vortices with azimuthal velocity profiles more like those used in previous studies give similar results.

1. Introduction

In recent years the dynamics of asymmetric disturbances in effectively two-dimensional swirling flows has been studied extensively due to their role in understanding phenomena in intense atmospheric vortices, such as hurricanes and tornadoes. Some of these applications to hurricane dynamics are the following: asymmetric disturbances to the storm potential vorticity field has been advanced as an explanation for the appearance of spiral rainbands (Guinn and Schubert 1993; Montgomery and Kallenbach 1997), in contrast to the earlier gravity wave theories (Kurihara 1976); asymmetric dynamics is used to explain both long- and short-term deviations of the hurricane track from that prescribed by the surrounding flow (Willoughby 1992, 1994; Smith

* Current affiliation: Department of Atmospheric Science, Colorado State University, Fort Collins, Colorado.

Corresponding author address: Dr. David S. Nolan, Department of Atmospheric Science, Colorado State University, Fort Collins, CO 80523.
E-mail: nolan@chandra.atmos.colostate.edu

and Weber 1993); and the rapid decay of higher-wavenumber disturbances in the vicinity of the vortex core helps explain the robustness of these storms to adverse influences, such as the beta effect and the shear of the environmental wind (Carr and Williams 1989; Smith and Montgomery 1995).

Asymmetric dynamics has long been of interest in the study of tornadoes since the realization that tornadoes sometimes contain several smaller vortices within the larger vortex core, and that the greatest damage is often found in the paths of these ''suction'' vortices (Fujita 1971). This phenomenon has been widely reproduced in both laboratory (Ward 1972; Church et al. 1979) and numerical models (Rotunno 1984; Lewellen 1993; Lewellen et al. 1997). In numerous studies addressing the linear stability of inviscid swirling flows (Rotunno 1978; Gall 1983, 1985; Staley and Gall 1979, 1984; Steffens 1988) and similar flows with viscosity (Staley 1985), instability of the vertical and azimuthal velocity field in the core of the tornado has been offered as an explanation for the appearance of ''multiple vortices.'' The general result has been to find instability for a finite range of low wavenumbers for two-dimensional instabilities, and a larger range of higher-wavenumber instabilities for three-dimensional (spiral) structures, which are identified as inertial instabilities (Leibovich and Stewartson 1983; Emanuel 1984). Interest in asymmetric tornado dynamics has been renewed by the discovery that three-dimensional models can sustain realistic tornado wind speeds (Lewellen et al. 1997; Fiedler 1998), while in the past axisymmetric models have not (Fiedler 1993, 1994; Nolan and Farrell 1999b). The higher wind speeds of the three-dimensional models have been associated with the simulated multiple vortices that appear in them, as Fujita (1971) anticipated for actual tornadoes.

A feature common to virtually all previous studies of vortex dynamics and stability has been neglect of the radial inflow that must be present to sustain the mean vortex flow against the effects of dissipation. This omission is due to the additional analytical difficulties brought on by the effects of radial advection on the perturbations and the fact that the presence of radial mean velocities makes the problem inherently nonseparable in most cases, that is, not susceptible to analyses with perturbations of the usual form $F(r)e^{i(k\theta+mz+\omega t)}$. Nolan and Farrell (1999a) were able to overcome these obstacles by constructing mean vortex flows with radial inflow for which initially two-dimensional perturbations remained strictly two-dimensional, and then by allowing the radial structure function of the perturbations to vary both temporally and radially. Two kinds of two-dimensional vortex flows were examined: one-celled vortices, where radial inflow penetrates all the way to the axis and the vortex core is in solid-body rotation, and two-celled vortices, where the radial inflow does not penetrate to the axis and the vortex core is stagnant. A change in sign of the mean-flow vorticity gradient in the two-celled vortex allows for modal instability in the range of azimuthal wavenumbers $3 \leq k \leq 10$, while the one-celled vortex was found to be stable for all wavenumbers. Furthermore, with the use of generalized stability theory (Farrell and Ioannou 1996) it was found that for both vortex types there was substantial transient growth in energy of optimally configured initial perturbations. Neglect of the dynamical terms associated with the radial inflow that sustains the mean vortex—the radial advection and the stretching terms—was shown to result in a large overestimation of transient growth in the one-celled vortex and also destabilization of azimuthal wavenumbers one and two in the two-celled vortex.

Nolan and Farrell (1999a) also investigated whether the eddy momentum fluxes associated with transiently growing disturbances cause a net tendency to increase or decrease the maximum wind speed of the mean vortex. While in most cases the net effect of introducing a disturbance is to increase the kinetic energy of the mean flow, the opposite result can be found in both one- and two-celled vortices for wavenumbers that have nearly neutral modes. In these cases, energy acquired from the mean flow during the growth stage of the disturbance was trapped in these nearly neutral modes and ultimately lost to dissipation, rather than being returned to the mean flow. Excitation of these nearly neutral modes was previously discussed by Smith and Montgomery (1995) in an analysis of evolving perturbations in an unbounded Rankine vortex, although they did not discuss their effect on the mean flow.

Transient growth of asymmetric disturbances in a vortex is a close analog to the transient growth phenomenon in linear shear flows originally demonstrated by Thompson (1887) and Orr (1907). This analogy has been further elucidated in discussions and examples by Smith and Montgomery (1995), Kallenbach and Montgomery (1995), and Nolan (1996). While the potential for substantial transient growth of properly configured initial disturbances certainly exists, Montgomery and Kallenbach (1997) have argued it is exceedingly unlikely to occur since the typical optimal initial condition for growth is a disturbance that is a tight, reverse spiral in the opposite direction of the flow, and there is no apparent mechanism to excite such disturbances in atmospheric vortices. Our work here will address this issue to some extent by exciting asymmetric perturbations in our mean vortex flows with forcing functions with no preferred spatial or temporal structure, so that we will answer the question: what role do these transiently growing disturbances play when the forcing lacks the bias of any specific forcing function? While this analysis may not necessarily apply to atmospheric vortices where only certain types of disturbances may be introduced, it will lend insight into the importance of including both radial inflow and transient growth in the analysis of asymmetric vortex dynamics.

A number of previous studies have used stochastic

analysis successfully to predict the eddy statistics of meteorological flows. The general technique is to linearize the evolution equations of small perturbations to a particular mean flow and then to augment these linear dynamics with stochastic forcing, which is uncorrelated in time (i.e., ''white noise'') and also possibly uncorrelated in space. Using this method, Farrell and Ioannou (1994, 1995) were successful in reproducing the observed variance of midlatitude disturbances and their associated heat fluxes. DelSole and Farrell (1996) showed that the eddy fluxes induced by stochastic forcing can be used to compute the equilibrium state of a fully nonlinear quasigeostrophic model of the midlatitude jet. More recently, Whitaker and Sardeshmukh (1998) used stochastic forcing to recover the observed variances of the winter Northern Hemisphere flow (in particular, the location and structure of the storm tracks) with considerable success.

Section 2 gives an introduction to the analysis of linear dynamical systems when they are excited by a stochastic forcing term. Section 3 will describe the two-dimensional vortex flows under consideration and give a brief description of how the evolution equations governing perturbations to this flow can be reduced to the form $d\mathbf{x}_k/dt = \mathbf{A}_k\mathbf{x}_k$ for each azimuthal wavenumber k. Section 4 describes the response of the vortices to the stochastic forcing, and section 5 investigates how this response feeds back onto the mean flow of the vortex through eddy momentum fluxes. Discussion of some of the important points are provided in section 6, and conclusions are presented in section 7.

2. Stochastically driven linear dynamical systems

An introduction to the theory of stochastic differential equations can be found in Gardiner (1985). Particular results for white-noise forcing have already been applied to the study of nonnormal shear flows, as discussed above, by Farrell and Ioannou (1993, 1994, 1995) and DelSole and Farrell (1996). We follow these authors' approach to solve directly for the response of a linear dynamical system driven by stochastic forcing with white-noise properties.

We begin by assuming our perturbation evolution equations have been reduced to a nonnormal linear dynamical system in generalized velocity coordinates [defined in (3.27) and (3.28); for examples of this procedure, see Farrell and Ioannou (1993), Delsole and Farrell (1996), and Nolan and Farrell (1999a)]. Now we add to the system a random forcing term $\mathbf{F}\boldsymbol{\xi}$:

$$\frac{d\mathbf{x}}{dt} = \mathbf{A}\mathbf{x} + \mathbf{F}\boldsymbol{\xi}. \tag{2.1}$$

The columns of the matrix operator $\mathbf{F}$ are a set of forcing functions, each separately driven randomly by the elements of the vector $\boldsymbol{\xi}(t)$. The elements of $\boldsymbol{\xi}(t)$ are complex Gaussian white-noise processes, having zero mean and unit covariance:

$$\langle \boldsymbol{\xi}_i(t) \rangle = 0 \tag{2.2}$$

and

$$\langle \boldsymbol{\xi}_i(t_1)\boldsymbol{\xi}_j^*(t_2) \rangle = \delta_{ij}\delta(t_1 - t_2), \tag{2.3}$$

where the brackets refer to ensemble averages and δ_{ij} is the Kronecker delta. The solution in time of (2.1) may be written as

$$\mathbf{x}(t) = e^{\mathbf{A}t}\mathbf{x}(0) + \int_0^t e^{\mathbf{A}(t-s)}\mathbf{F}\boldsymbol{\xi}\, ds. \tag{2.4}$$

The first term on the rhs of (2.4) refers to the evolution of the initial conditions, which decay to zero when all the eigenvalues of $\mathbf{A}$ have a negative real part. Since this is true for all of the systems considered here, we can ignore this term in subsequent analyses, which focus on steady states achieved as $t \to \infty$. The second term is the accumulated effect of all of the forcings from $t = 0$ to the present time t.

Recalling that in generalized velocity coordinates the energy of the system is $E = \mathbf{x}^*\mathbf{x}$, one can directly solve for the ensemble average energy of the perturbations as a function of time:

$$\begin{aligned}\langle E^t \rangle &= \langle \mathbf{x}^*(t)\mathbf{x}(t) \rangle \\ &= \left\langle \int_0^t ds \int_0^t \xi^*(s)\mathbf{F}^\dagger e^{\mathbf{A}^\dagger(t-s)} e^{\mathbf{A}(t-s')}\mathbf{F}\boldsymbol{\xi}(s')\, ds' \right\rangle \\ &= \mathrm{trace}\left[\mathbf{F}^\dagger\left(\int_0^t e^{\mathbf{A}^\dagger(t-s)}e^{\mathbf{A}(t-s)}\, ds\right)\mathbf{F}\right] \\ &= \mathrm{trace}[\mathbf{F}^\dagger\mathbf{B}^t\mathbf{F}],\end{aligned} \tag{2.5}$$

where we have made use of the properties (2.2) and (2.3) of the forcing terms and defined the Hermitian operator $\mathbf{B}^t$ as

$$\mathbf{B}^t = \int_0^t e^{\mathbf{A}^\dagger(t-s)}e^{\mathbf{A}(t-s)}\, ds. \tag{2.6}$$

Thus we can see that the energy of the system depends both on the dynamics of the system as represented in $\mathbf{A}$ and on the structures and magnitudes of the forcing functions in $\mathbf{F}$. Note that an eigenvalue decomposition of $\mathbf{B}^t$ will provide a set of functions ordered in the extent to which they would excite the system at time t as forcing functions, with their relative responses described by their positive definite eigenvalues. These forcing functions are referred to as stochastic optimals (SOs).

With some manipulation we can solve for the steady-state solution of (2.5). Differentiating (2.6) with respect to the time t, we find a time evolution equation for $\mathbf{B}^t$:

$$\frac{d\mathbf{B}^t}{dt} = \mathbf{I} + \mathbf{A}^\dagger\mathbf{B}^t + \mathbf{B}^t\mathbf{A}, \tag{2.7}$$

where $\mathbf{I}$ is the identity matrix. We would like to find $\mathbf{B}^\infty$ without having to directly evaluate $\lim_{t\to\infty}\mathbf{B}^t$. Since all

the eigenvalues of $\mathbf{A}$ have negative real part, as $t \to \infty$ the system achieves a statistically steady state and the time rate of change must go to zero, so

$$\mathbf{A}^\dagger \mathbf{B}^\infty + \mathbf{B}^\infty \mathbf{A} = -\mathbf{I}. \tag{2.8}$$

An equation of this form is known as a Lyapunov equation and can be solved by standard methods (Lefschetz 1963; DelSole 1993). Eigenvector decomposition of $\mathbf{B}^\infty$ provides the SOs for the system when it has reached a steady state.

Through a very similar procedure we can find the structures that represent an ordered decomposition of the response of the system to the stochastic forcing, usually referred to as empirical orthogonal functions (EOFs). To find the EOFs, we need the full correlation matrix of the system:

$$\begin{aligned} \mathbf{C}^t_{ij} &= \langle \mathbf{x}_i(t)\mathbf{x}^*_j(t)\rangle \\ &= \left\langle \int_0^t ds \int_0^t e^{\mathbf{A}(t-s)}\mathbf{F}\boldsymbol{\xi}\boldsymbol{\xi}^*\mathbf{F}^\dagger e^{\mathbf{A}(t-s)}\, ds \right\rangle \\ &= \left(\int_0^t e^{\mathbf{A}(t-s)}\mathbf{H}e^{\mathbf{A}^\dagger(t-s)}\, ds \right)_{ij}, \end{aligned} \tag{2.9}$$

where we have written $\mathbf{H} = \mathbf{F}\mathbf{F}^\dagger$. When $\mathbf{F}$ is unitary, $\mathbf{H} = \mathbf{I}$; therefore, all unitary forcing operators result in the same response. By differentiating (2.9) we obtain an evolution equation for the correlation matrix:

$$\frac{d\mathbf{C}^t}{dt} = \mathbf{H} + \mathbf{A}\mathbf{C}^t + \mathbf{C}^t\mathbf{A}^\dagger, \tag{2.10}$$

and we can also find the steady-state solution in terms of a Lyapunov equation:

$$\mathbf{A}\mathbf{C}^\infty + \mathbf{C}^\infty\mathbf{A}^\dagger = -\mathbf{H} \tag{2.11}$$

(this equation is also known as the fluctuation–dissipation relation).

The decomposition of the full correlation matrix (2.9) into its EOFs is known as the Karhunen–Loeve (K–L hereafter) decomposition (Loeve 1978), while the decomposition of the space of forcing functions into orthogonal functions ordered by their contribution to the variance has been called the ''back K–L decomposition'' by Farrell and Ioannou (1993). Observe that when the forcing is unitary so that $\mathbf{H} = \mathbf{I}$, Eqs. (2.8) and (2.11) for the SOs and the EOFs have a certain antisymmetry. On the other hand, when the dynamical operator $\mathbf{A}$ is normal, the eigenfunctions of both $\mathbf{B}^\infty$ and $\mathbf{C}^\infty$ reduce to the complete and orthogonal eigenfunctions of $\mathbf{A}$. In this case the response of the system can be entirely predicted and interpreted in terms of these eigenfunctions, or normal modes, of $\mathbf{A}$. (In fact, each normal mode would behave like a stochastically forced damped harmonic oscillator, independently of the other modes.) When $\mathbf{A}$ is not normal, as in the case of our vortex flows, the forcing functions and response functions differ in a manner analogous to the difference between the least damped modes and the least damped modes of the adjoint operator $\mathbf{A}^\dagger$ (e.g., see Farrell 1988; DelSole and Farrell 1996; Nolan and Farrell 1999a). The fact that the EOFs of a nonnormal system are distinct from the modes of the dynamical operator is discussed by North (1984).

Finally, we note that the average perturbation energy can be found from both the forcing matrix and the response matrix:

$$E^\infty = \text{trace}\{\mathbf{C}^\infty\} = \text{trace}\{\mathbf{F}^\dagger\mathbf{B}^\infty\mathbf{F}\}, \tag{2.12}$$

while the energy input from the stochastic forcing is

$$E_{\text{in}} = \text{trace}(\mathbf{F}^\dagger\mathbf{F}) = N, \tag{2.13}$$

when $\mathbf{F}$ is unitary with rank N.

3. Two steady-state vortex flows and equations for the evolution of asymmetric perturbations

In this section we briefly describe the dynamics of the one- and two-celled vortices. We also derive equations of motion for two-dimensional, asymmetric perturbations and reduce them to the form of a linear dynamical system $d\mathbf{x}/dt = \mathbf{A}\mathbf{x}$. For more details and discussion, see Nolan and Farrell (1999a).

a. The one-celled vortex

We wish to find a steady-state solution for the azimuthal velocity field sustained by a fixed cylindrical deformation field, which is analogous to the Burgers' vortex solution (Burgers 1948; Rott 1958) but is contained in a closed domain. We define a cylindrically symmetric radial velocity function that is fixed in time as

$$U = U(r). \tag{3.1}$$

By continuity, we have

$$\frac{\partial W}{\partial z} = -\frac{1}{r}\frac{\partial}{\partial r}(rU), \tag{3.2}$$

so that the vertical velocity field $W(r, z)$ may be determined up to constant. Holding the U and W velocities fixed, we can write down a single advection–diffusion equation for the evolution of the axisymmetric azimuthal velocity $V(r)$:

$$\frac{\partial V}{\partial t} + U\frac{\partial V}{\partial r} + \frac{UV}{r} = \nu\left(\frac{\partial^2 V}{\partial r^2} + \frac{1}{r}\frac{\partial V}{\partial r} - \frac{V}{r^2}\right). \tag{3.3}$$

We use a cylindrically symmetric deformation field similar to the Burgers' vortex deformation field, except that its support lies entirely within a cylinder of radius $r = b = 7$. Furthermore, we require that the radial inflow velocity transitions smoothly to zero as we approach the outer boundary and is nearly zero for a substantial region near the outer boundary. Such a radial inflow function is given by

$$U(r) = -\alpha r e^{-\mu r^6}. \tag{3.4}$$

This function with $\alpha = 5.0 \times 10^{-3}$ and $\mu = 2.44 \times 10^{-4}$ is shown in Fig. 1a. This particular choice for α, in conjunction with a choice of $\nu = 0.001$ for the viscosity, sets the radius of maximum winds RMW = 1 for the well-known Burgers' vortex solution (see Burgers 1948; Rott 1958). Using this radial velocity field and an outer boundary condition on V such that the circulation at the outer boundary $\Gamma_b = 2\pi r_b V_b = 2\pi$ (i.e., the circulation of the fluid at the edge of the domain is equal to 2π everywhere), (3.3) results in the solution shown in Fig. 1b. The *vortex Reynolds number* is $\mathrm{Re}_V = r_b V_b/\nu = 1000$. This solution, which has RMW = 1.0 and maximum azimuthal wind speed $V_{\max} = 0.71$, is virtually identical to the Burgers' solution with the same parameters, despite the fact that the radial inflow velocity transitions to zero near the outer edge of the domain. The deformation (or negative horizontal divergence) of the radial velocity function is shown in Fig. 1c, while the radial gradient of the vertical component of vorticity is shown in Fig. 1d.

b. Two-celled vortices

A simple model of a two-celled vortex is obtained by defining the radial velocity $U(r)$ to have inflow outside some radius, and outflow away from the $r = 0$ axis, with a stagnation point in between:

$$U(r) = \begin{cases} 0, & r < 0.2 \\ 0.02 \sin^2\left(\pi \dfrac{r - 0.2}{1.6}\right), & 0.2 < r < 1 \\ 0.035 \cos\left(\pi \dfrac{r - 1}{2.0}\right) - 0.15, & 1 < r < 3 \\ -0.05 \cos^2\left(\pi \dfrac{r - 3}{7.0}\right), & 3 < r < 6.5 \\ 0, & r > 6.5. \end{cases} \tag{3.5}$$

This radial velocity function is shown in Fig. 2a. In previous work, Nolan and Farrell (1999a) used this radial velocity field and a viscosity of $\nu = 0.001$ to produce a two-celled vortex with a completely stagnant core ($V \cong 0$ for $r < 1.2$); however, that vortex is unstable for azimuthal wavenumbers $3 \leq k \leq 10$. Since we cannot study the stationary statistics of a linear dynamical system with an unstable operator $\mathbf{A}$, we instead increase the viscosity until the vortex is marginally stable for all wavenumbers; this has the side effect of smoothing the resultant azimuthal velocity field so that it is nonzero in the vortex core. The smallest viscosity that stabilizes this two-celled vortex for all azimuthal wavenumbers was found to be $\nu = 0.0058$. Applying our method with this higher viscosity, where again we have defined the circulation at the outer boundary $\Gamma_b = 2\pi$, we find the azimuthal velocity profile shown in Fig. 2b. In this case RMW = 2.19 and $V_{\max} = 0.43$. The associated deformation function is shown in Fig. 2c, while the resulting vertical vorticity gradient is shown in Fig. 2d. Outside RMW the velocity profile is nearly that of a potential flow. A stability diagram for this modified two-celled vortex is shown in Fig. 3, along with the stability curve for an identical azimuthal velocity profile with the radial inflow terms neglected in the perturbation dynamics. Neglect of the radial inflow, which sustains the mean vortex circulation, nearly destabilizes the two-celled vortex for azimuthal wavenumber $k = 1$ (decay rate 1.1×10^{-4}) and does destabilize the vortex for $k = 2$ and $k = 3$.

c. Dimensional interpretation of the nondimensional results

To interpret the results that follow in later sections, the dimensionless variables may be rescaled in terms of dimensional velocity, length, and timescales, that is,

$$r^* = Lr, \tag{3.6}$$

$$(u^*, v^*) = U(u, v), \tag{3.7}$$

$$t^* = Tt, \tag{3.8}$$

where (*) indicates dimensional variables. For application of the dimensionless results to a particular physical case, the dimensional scalings L and U must be chosen so that RMW and the maximum azimuthal wind speed ($V_{\max}$) correspond to those of the physical problem when the variables are rescaled according to (3.6)–(3.8). For example, suppose we wanted to apply the results of an analysis of the two-celled vortex to a hurricane with a maximum wind speed of 40 m s^{-1} and an RMW of 20 km. The dimensional scalings must be chosen so that the dimensionless values of the RMW and $V_{\max}$ are rescaled to those of the physical problem:

$$L = \frac{\mathrm{RMW}^*}{\mathrm{RMW}} = \frac{20 \text{ km}}{2.19} = 9.13 \text{ km} \tag{3.9}$$

$$U = \frac{V^*_{\max}}{V_{\max}} = \frac{40 \text{ m s}^{-1}}{0.43} = 93 \text{ m s}^{-1}. \tag{3.10}$$

The natural choice for the timescale is the advective time $T = L/U$; for the example here $T = 98$ s. The timescale is necessary for physical interpretation of the decay rates of the least damped modes or the for time when a global optimal reaches its maximum energy. As an example, let us take the results for the two-dimensional vortex with and without radial inflow, as described in the previous section (see also Fig. 3), and rescale them for this example of a hurricane. We find that the timescale τ for decay (equal to the inverse of the decay rate) of the wavenumber 1 least damped mode is $\tau = 5.4 \times 10^3$ s (1.5 h) when radial inflow is included,

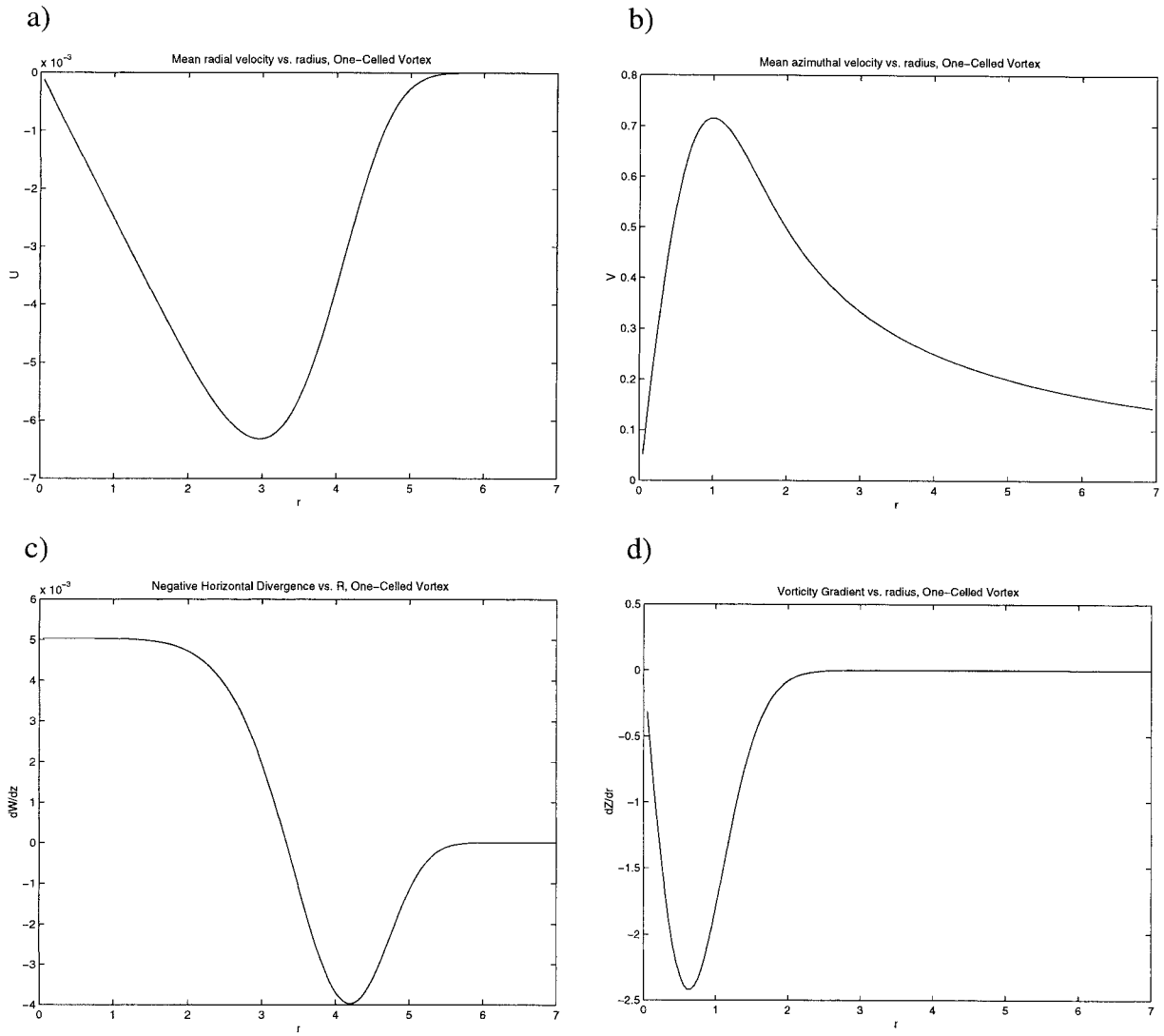

FIG. 1. Profiles of radial and and azimuthal velocity for the one-celled vortex: (a) radial velocity, (b) azimuthal velocity, (c) negative horizontal divergence (stretching), and (d) vorticity gradient.

but instead is $\tau = 8.9 \times 10^5$ s (247 h) when the radial inflow is neglected.

d. The evolution of vertical vorticity perturbations

We restrict our attention to the dynamics of the vertical vorticity component ζ in cylindrical coordinates. This vertical vorticity component is assumed to have no variation in the vertical direction and its dynamics are governed by

$$\frac{\partial \zeta}{\partial t} + u\frac{\partial \zeta}{\partial r} + \frac{v}{r}\frac{\partial \zeta}{\partial \theta} = \zeta\frac{\partial w}{\partial z} + \nu\left(\frac{\partial^2 \zeta}{\partial r} + \frac{1}{r}\frac{\partial \zeta}{\partial r} + \frac{1}{r^2}\frac{\partial^2 \zeta}{\partial \theta}\right). \tag{3.11}$$

We write each term in (3.11) as the sum of a radially varying mean and azimuthally, radially, and temporally varying perturbations: $u = U(r) + u'(r, \theta, t)$, $\zeta = Z(r) + \zeta'(r, \theta, t)$, and similarly for v and w. We can then separate the solutions by writing them as a sum of harmonically varying azimuthal waves, that is, $\zeta'(r, \theta, t) = \Sigma_k \zeta_k(r, t)e^{ik\theta}$, and so on for the perturbations of u and v also. Substituting these forms into (3.11), we obtain for each wavenumber k a linear equation for the evolution of the radially and temporally varying vorticity function $\zeta_k(r, t)$:

$$\left[\frac{\partial}{\partial t} + U(r)\frac{\partial}{\partial r} + ik\Omega(r)\right]\zeta_k + u_k\frac{\partial Z}{\partial r} = \zeta_k\frac{\partial W}{\partial z} + \nu\left(\frac{\partial^2 \zeta_k}{\partial r^2} + \frac{1}{r}\frac{\partial \zeta_k}{\partial r} - \frac{k^2}{r^2}\zeta_k\right). \tag{3.12}$$

From here on we will use the convention that the terms

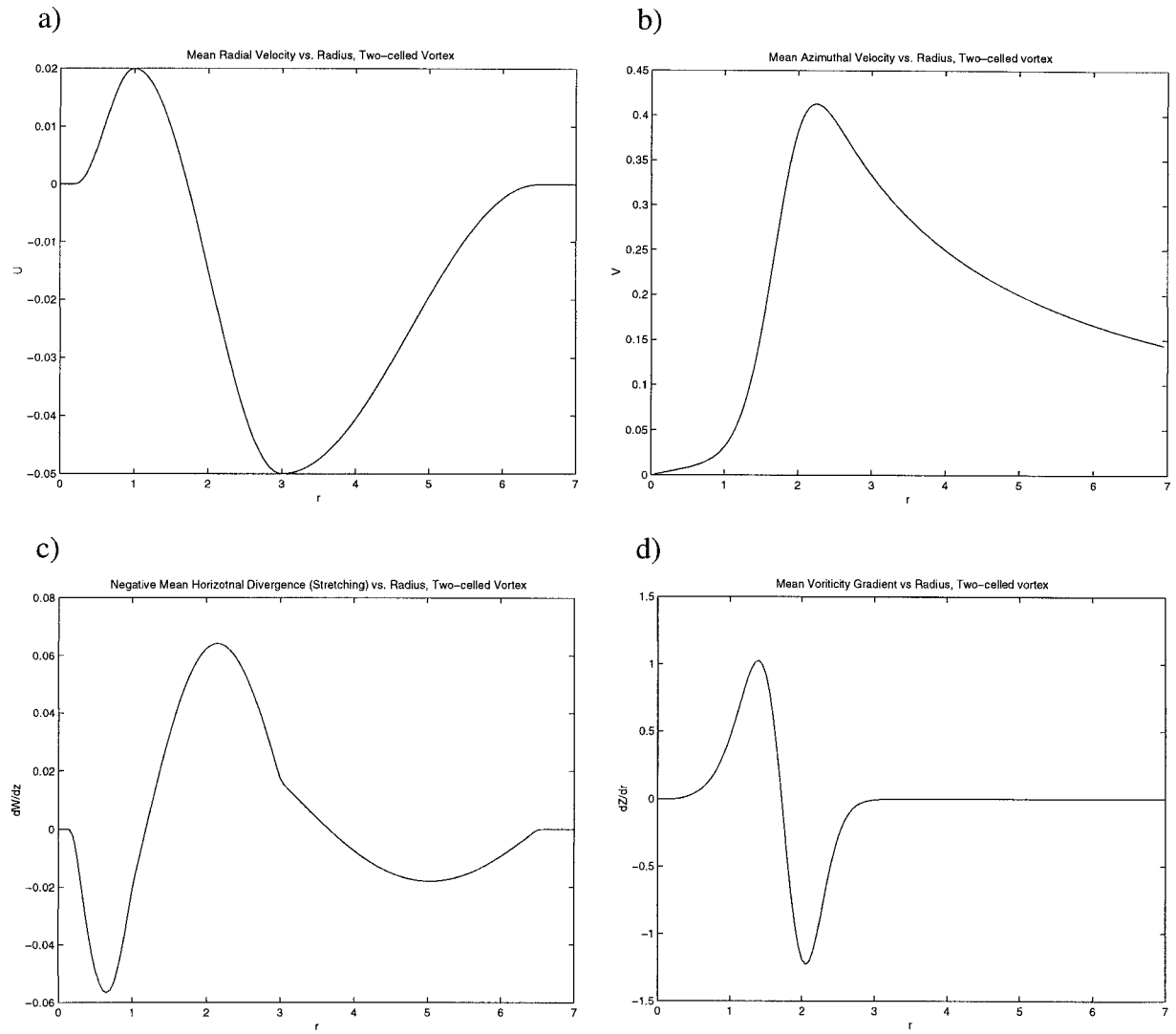

FIG. 2. Profiles of radial and and azimuthal velocity for the two-celled vortex: (a) radial velocity, (b) azimuthal velocity, (c) negative horizontal divergence (stretching), and (d) vorticity gradient.

u_k, v_k, ζ_k refer to complex amplitude functions of r and t only.

As seen in (3.12), when there is a nonzero background vorticity gradient $\partial Z/\partial r$, obtaining the evolution of the perturbation vorticity requires knowledge of the radial velocity perturbations. Following Carr and Williams (1989) and Smith and Montgomery (1995), we find the velocities by solving for the perturbation streamfunction:

$$\psi(r,\ \theta,\ t) = \sum_k \psi_k(r,\ t)e^{ik\theta}, \tag{3.13}$$

$$u_k = -\frac{1}{r}\frac{\partial \psi_k}{\partial \theta} = \frac{-ik}{r}\psi_k, \quad \text{and} \tag{3.14}$$

$$v_k = \frac{\partial \psi_k}{\partial r}. \tag{3.15}$$

We choose the boundary conditions so that there is no normal flow at the outer boundary $r = b$, that is,

$$\psi_k(0,\ t) = \psi_k(b,\ t) = 0. \tag{3.16}$$

Given the vorticity, the streamfunction may be found with a Green's function:

$$\psi_k(r,\ t) = \int_a^b G_k(r,\ \rho)\zeta_k(\rho,\ t)\ d\rho. \tag{3.17}$$

The Green's function appropriate for this problem is (Carr and Williams 1989)

$$G_k(r,\ \rho) = \begin{cases} \dfrac{r^{2k}}{2kr^k b^{2k}}(\rho^{k+1} - b^{2k}\rho^{-k+1}), & 0 \le r \le \rho \\ \dfrac{r^{2k} - b^{2k}}{2kr^k b^{2k}}\rho^{k+1}, & \rho \le r \le b. \end{cases} \tag{3.18}$$

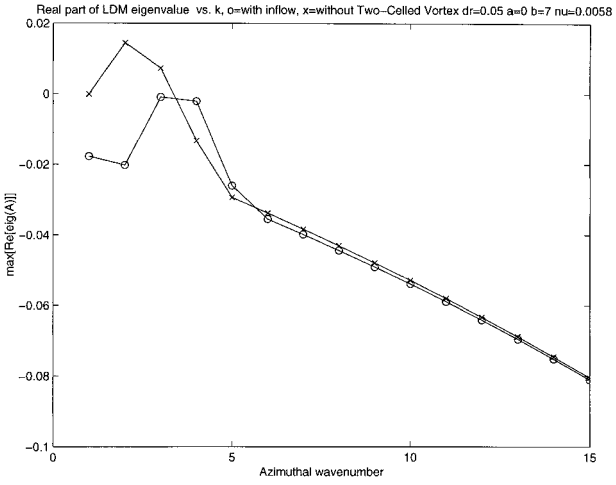

FIG. 3. The real part of the least damped mode as a function of azimuthal wavenumber (stability diagram) for the two-celled vortex; ○'s: with the radial inflow effects included in the perturbation dynamics; ×'s: with the radial inflow effects negelected.

e. Reduction to a linear dynamical system in generalized velocity coordinates

We would like to find the linear dynamical system in matrix form that governs the evolution of the vorticity perturbations. We discretize the domain by assigning the values of the radial functions to evenly spaced points from $r = 0 + \Delta r$ to $r = b - \Delta r$, where each point is separated by a distance Δr. This converts the continuous radial functions into vectors of length $N = (b/\Delta r) - 1$. For most calculations presented here we use $\Delta r = 0.05$ so that $N = 139$. We express all derivatives as matrix operators corresponding to the usual centered-difference approximations, with the exception that the finite-difference operator used for the advection term is one-sided, representing a second-order upwinding advection scheme (this was necessary to preserve numerical stability). We must also express the Green's function operation (3.17) as a matrix operation, that is,

$$\psi_k = \mathbf{G}_k \zeta_k. \tag{3.19}$$

Finally, the vorticity evolution equation (3.12) is put in matrix dynamical system form with only the time derivative on the lhs:

$$\frac{d\zeta_k}{dt} = \mathbf{T}_k \zeta_k \tag{3.20}$$

with

$$\mathbf{T}_k = -\mathbf{U}\mathbf{D}_{\text{up}} - ik\boldsymbol{\Omega} + (\mathbf{D}\mathbf{Z})ik\mathbf{R}^{-1}\mathbf{G}_k + \mathbf{S} + \nu(\mathbf{D}^2 + \mathbf{R}^{-1}\mathbf{D} - k^2\mathbf{R}^{-2}). \tag{3.21}$$

Where we have written $\mathbf{D}$ for the matrix representing the finite-difference derivative with respect to r, $\mathbf{D}_{\text{up}}$ for a similar but second-order upwinded derivative operator, $\mathbf{R}$ for the radius, and $\mathbf{S}$ for the "stretching" term $\partial W/\partial z$. We must also incorporate into these difference operators additional boundary conditions on the vorticity, which we choose to be

$$\zeta_k(0) = \zeta_k(b) = 0. \tag{3.22}$$

This condition minimizes the effects of the outer boundaries on the interior dynamics.

The kinetic energy of each perturbation is

$$E = \int_0^b \left(\frac{\overline{u_k^2}}{2} + \frac{\overline{v_k^2}}{2}\right) 2\pi r\, dr = -\frac{1}{2}\int_0^b \overline{\psi_k \zeta_k}\, 2\pi r\, dr = -\frac{\pi}{4}\int_0^b (\psi_k^* \zeta_k + \zeta_k^* \psi_k) r\, dr, \tag{3.23}$$

where the overbars refer to azimuthal averages of the real parts of the complex functions. We define an energy metric operator $\mathbf{M}$ such that the energy of our discretized linear dynamical system is written $E = \zeta^* \mathbf{M} \zeta$. For each azimuthal wavenumber k the energy metric can be formulated from (3.23)

$$\mathbf{M}_k = \frac{-\pi \Delta r}{4}[\mathbf{G}_k^\dagger \mathbf{R} + \mathbf{R}\mathbf{G}_k]. \tag{3.24}$$

By the additional transformations,

$$\mathbf{x}_k = \mathbf{M}_k^{1/2} \zeta_k \quad \text{and} \tag{3.25}$$

$$\mathbf{A}_k = \mathbf{M}_k^{1/2} \mathbf{T}_k \mathbf{M}_k^{-1/2}, \tag{3.26}$$

the system is converted into *generalized velocity coordinates*, so that the dynamics are expressed in the canonical form

$$\frac{d\mathbf{x}_k}{dt} = \mathbf{A}_k \mathbf{x}_k \quad \text{and} \tag{3.27}$$

$$E = \mathbf{x}_k^* \mathbf{x}_k. \tag{3.28}$$

4. Stochastic forcing of inflow-driven vortices: System response

In this section we will use the techniques described in section 2 to solve directly for the variance of stochastically driven perturbations in our one- and two-celled vortices. We will also use the K–L decomposition and back K–L decomposition to find the structures that contain most of the variance (the EOFs), and also the forcing functions that result in the most variance (the SOs). The effect of inflow velocity on the variance is also shown.

a. Response to stochastic forcing of the one-celled vortex

Figure 4 shows contour plots of the vorticity and streamfunction fields of the primary SOs for $k = 1$ and $k = 2$ in the one-celled vortex, which contribute 66% of the variance and 24% of the variance, respectively. These perturbations are similar and have two important

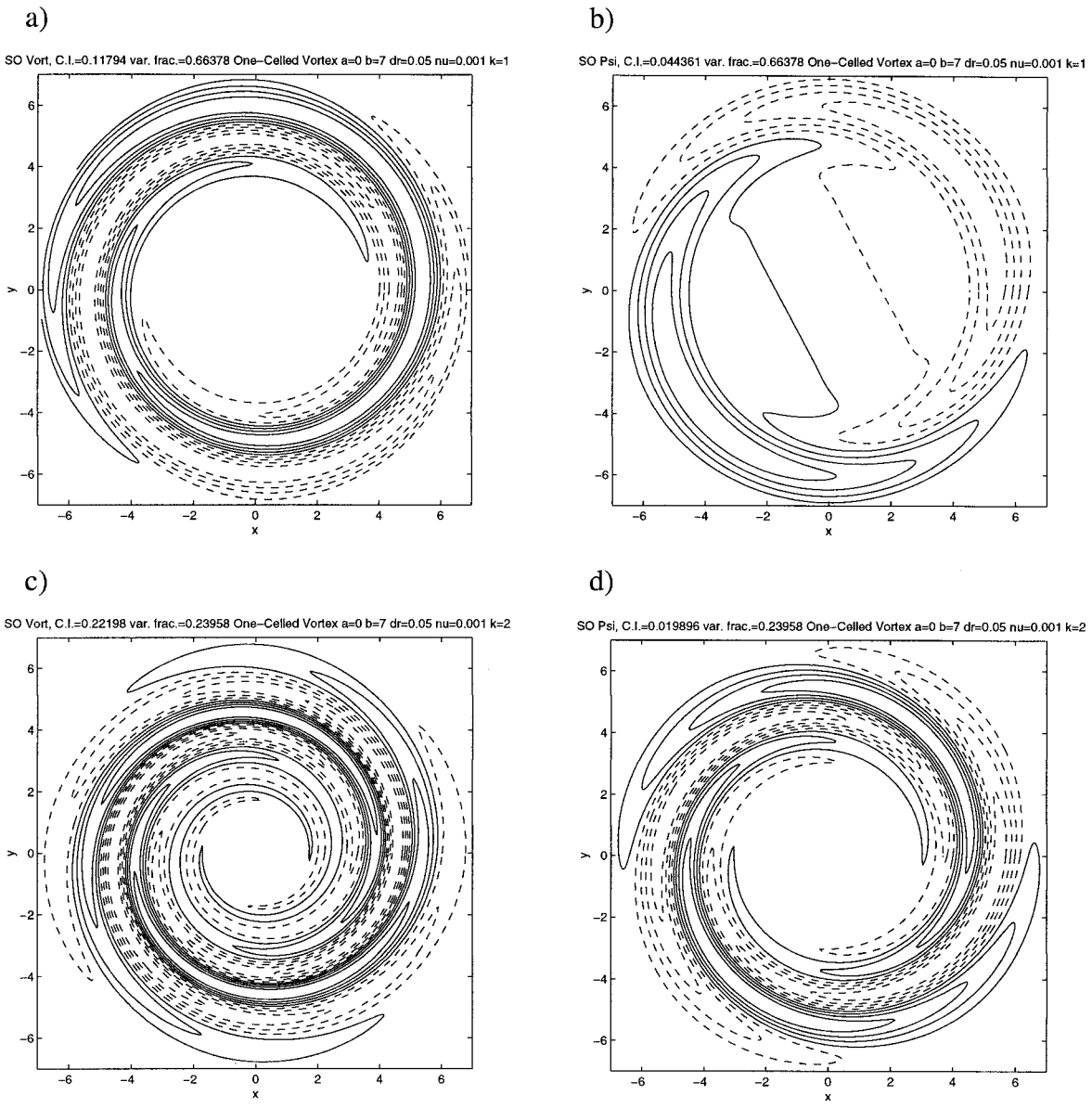

FIG. 4. Stochastic optimals (SOs) for $k = 1$ and $k = 2$ in the one-celled vortex: (a) $k = 1$ vorticity, (b) $k = 1$ streamfunction, (c) $k = 2$ vorticity, and (d) $k = 2$ streamfunction. Their fractional contribution to the variance is listed at the top of each plot, where the contour interval is also indicated. Negative contours are dashed.

features: 1) they are structures that spiral back against the flow of the vortex, and 2) they are displaced from the core of the vortex with their maximum vorticities and streamfunctions near $r = 5$. These two features are indicative of how a perturbation must be initially configured so as to maximize the energy it acquires from the mean flow, as has previously been demonstrated by Nolan and Farrell (1999a) for vortex flows with radial inflow. Such perturbations must spiral back against the vortex flow so that they are everywhere locally tilted back against the shear of the mean flow, and they must lie outside the vortex core so that they will be not be swept into the vortex core before they can maximize their wave–mean flow interactions.

This point is emphasized by comparison with Figs. 6a, b, which show the vorticity and streamfunction fields for the $k = 1$ global optimal for the one-celled vortex. The global optimal is the perturbation that grows the most in energy (in this case, by a factor of 209), and its growth is one measure of the potential for wave–mean flow interaction in a particular mean flow. The strong similarity between the stochastic optimal and the global optimal shows that the extent to which stochastic forcing excites transient growth of perturbations is

closely related in this example to the extent to which the stochastic forcing projects onto the global optimals.

We can also find the dominant perturbation structures that result from the stochastic forcing, as described in section 2. This system response depends on the structure of the forcing functions in the columns of the matrix **F** as shown in (2.9), but it is the same for all unitary **F**. When **F** is unitary we are forcing all resolved scales equally in energy. Using such a unitary set of forcing functions and normalizing the rate of energy input to one [see (2.13)], we obtain the primary EOFs for $k = 1$ and $k = 2$ in the one-celled vortex, which represent 98% and 43% of the variance, respectively, as shown in Fig. 5. For the same reasons that the primary SOs were very similar to the global optimals, these structures are very similar to the *realizations* of the global optimals, which are shown in Figs. 6c,d. The realizations of the global optimals are the structures that the global optimals assume when they obtain their maximum energy as they are deformed by the mean flow. As a general principle, this maximum energy is achieved when the vorticity has been arranged into the most compact structure achievable under the mean-flow dynamics, an arrangement that maximizes its associated square velocities and therefore its kinetic energy. The strong similarity between the EOFs and the realizations of the global optimals again emphasizes that the transfer of energy from the mean flow to perturbations is dominated by excitation of the global optimals. Furthermore, the fact that the $k = 1$ primary EOF represents so much (98%) of the variance is caused by the close similarity between the realization of the global optimal and the least damped mode (see Nolan and Farrell 1999a); when growing structures reach their maximum energy, their energy is trapped in the nearly neutral least-damped mode, which in this case has a decay rate of 2.0×10^{-3} (i.e., the timescale for decay is 79.6 revolutions of the mean vortex). The least damped mode for $k = 1$ in the one-celled vortex is a slightly modified version of the ''pseudomode,'' which for unbounded vortices is a wavenumber of one perturbation whose streamfunction is proportional to the mean flow velocity (Michaelke and Timme 1967; Gent and McWilliams 1986). Such a perturbation simply represents a linear displacement of the center of the vortex, which is why it decays so slowly, and again contributes to the dominance of the primary EOF in the response. For higher wavenumbers the realizations of the global optimals and the least damped modes are not similar in structure.

b. Response to stochastic forcing of the two-celled vortex

Figure 7 shows the primary SOs for $k = 1$ and $k = 3$ in the two-celled vortex, which represent 61% and 98% of the contribution to the excitation of the variance, respectively. These structures are very similar to the SOs for the one-celled vortex, with the exception that they have vorticity in the vortex core because vorticity is being advected outward from the center axis as well as inward from the outer boundary. We again see the similarity between the SOs and the global optimals, as shown for $k = 3$ in the two-celled vortex in Figs. 9a,b. The primary EOFs for $k = 1$ and $k = 3$ in the two-celled vortex, as shown in Fig. 8, represent 76% and 98% of the variance under unitary stochastic forcing. They again have structures similar to the realizations of the global optimals, which are shown for $k = 3$ in Figs. 9c,d. Therefore, we conclude that the wave–mean flow interactions are dominated by the excitation of the global optimals in the two-celled vortex as well.

Note, however, that in the case of the two-celled vortex, both the realizations of the global optimals and the EOFs for this wavenumber are not like the symmetric, coherent structures that we saw above for the one-celled vortex, but rather they are very close approximations to the least damped modes (not shown), which are structures that sustain themselves by converting mean-flow vorticity to perturbation vorticity. Thus, instead of being sheared over by the mean flow, the global optimal evolves into a nearly neutral structure that persists for long times. Further discussion of this point may be found in Nolan and Farrell (1999a).

c. Sustained variance and the effects of radial inflow

The total variance sustained by the stochastic forcing of the system can be found as in (2.12). In flows with strong shear, this variance greatly exceeds that estimated by equating the rate of energy input to the modal dissipation rate, which, assuming all modes are stable and equally excited (as in the case of unitary **F**), would be

$$E^{\infty}_{\text{modal}} = \frac{1}{N} \sum_{i=1}^{N} \frac{1}{(\lambda_i + \lambda_i^*)}, \tag{4.1}$$

where the λ_i are the eigenvalues of **A**, N is the dimension of the system, and the rate of energy input has been normalized to be equal to one. Such a calculation is correct for a dynamical system with a normal operator **A** (such as a set of damped harmonic oscillators), but it is incorrect for nonnormal systems, such as those representing fluid flows with shear. In this case the sustained variance is usually much greater than that computed from (4.1), and, in fact, Iouannou (1995) showed rigorously that the correctly computed variance (2.12) is always greater than that estimated from the dissipation rates of the modes:

$$E^{\infty} = \text{trace}[\mathbf{C}^{\infty}] \geq E^{\infty}{}_{\text{modal}}, \tag{4.2}$$

with equality occurring only when **A** is normal. The increased variance in shear flows is due to transiently growing disturbances, which acquire energy from the mean flow.

Figure 10 shows the variance under stochastic forcing with unitary **F**, normalized to one unit of energy input per unit time, as a function of azimuthal wavenumber

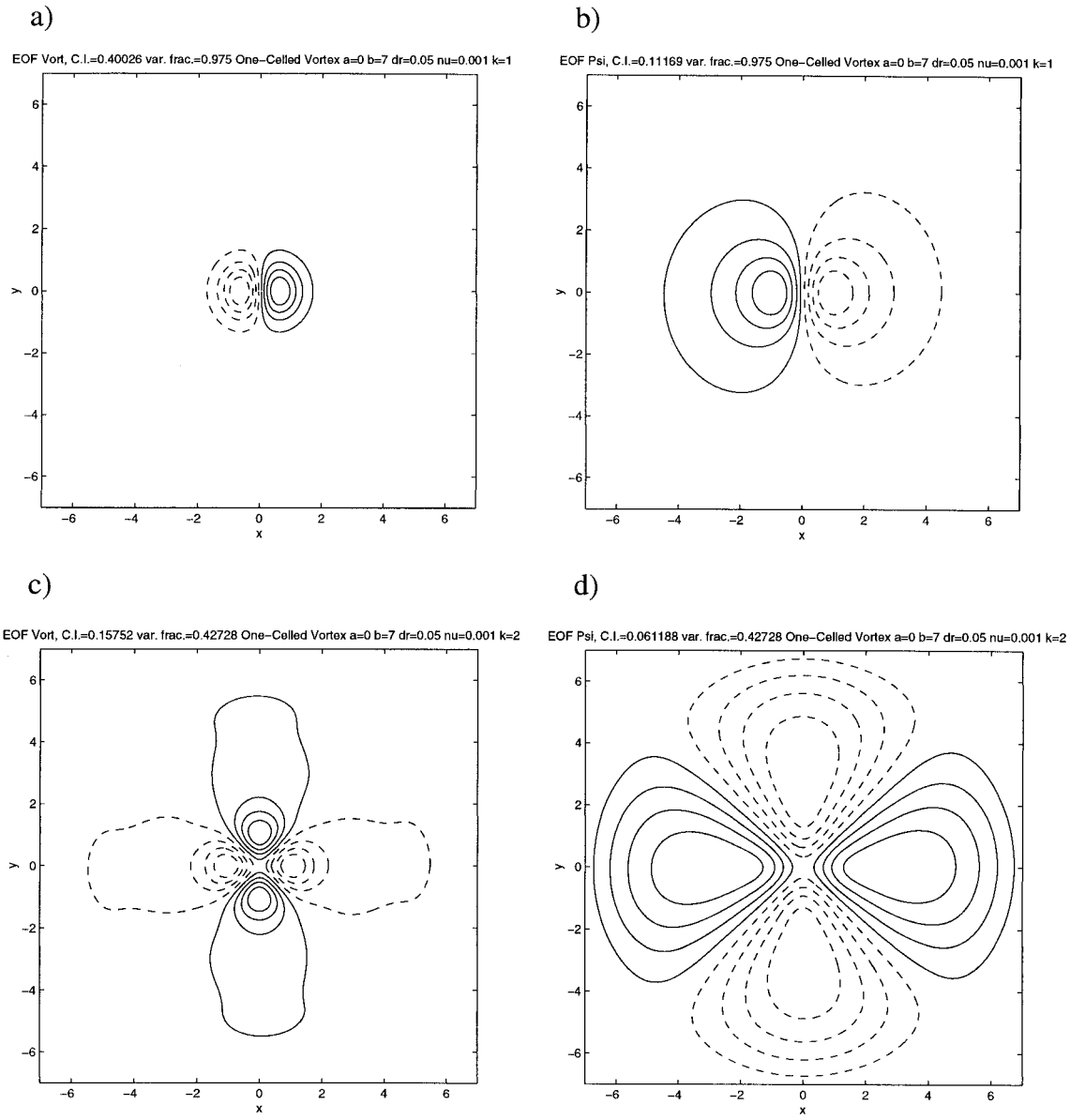

FIG. 5. EOFs for $k = 1$ and $k = 2$ in the one-celled vortex: (a) $k = 1$ vorticity, (b) $k = 1$ streamfunction, (c) $k = 2$ vorticity, and (d) $k = 2$ streamfunction. Their fractional representation of the variance is listed at the top of each plot, where the contour interval is also indicated. Negative contours are dashed.

in the one and two vortices. For each vortex we have plotted the variance in three different cases: 1) the variance computed from (4.2); 2) this same variance but with the radial inflow terms [$\mathbf{S}$ and $-\mathbf{UD}_{up}$ in (3.21)] neglected in the perturbation dynamics; and 3) the variance of an ''equivalent normal'' system, that is, that calculated from (4.1). For both vortices the actual variance is about an order of magnitude larger than the equivalent normal variance at all wavenumbers. Second, with the exceptions of $k = 4$ and $k = 5$ for the two-celled vortex, in all cases the variance is larger when the radial inflow is neglected, although only by a small percentage for $k > 1$ in the one-celled vortex and $k > 5$ in the two-celled vortex.

5. Momentum fluxes and mean flow deviations

We have established that stochastic excitation of asymmetric disturbances in the vortices we are studying leads to excitation of transiently growing perturbations that contribute greatly to the sustained perturbation variance, and that for wavenumbers with nearly neutral modes the effect of including radial inflow is to suppress these perturbations and their associated variance. How-

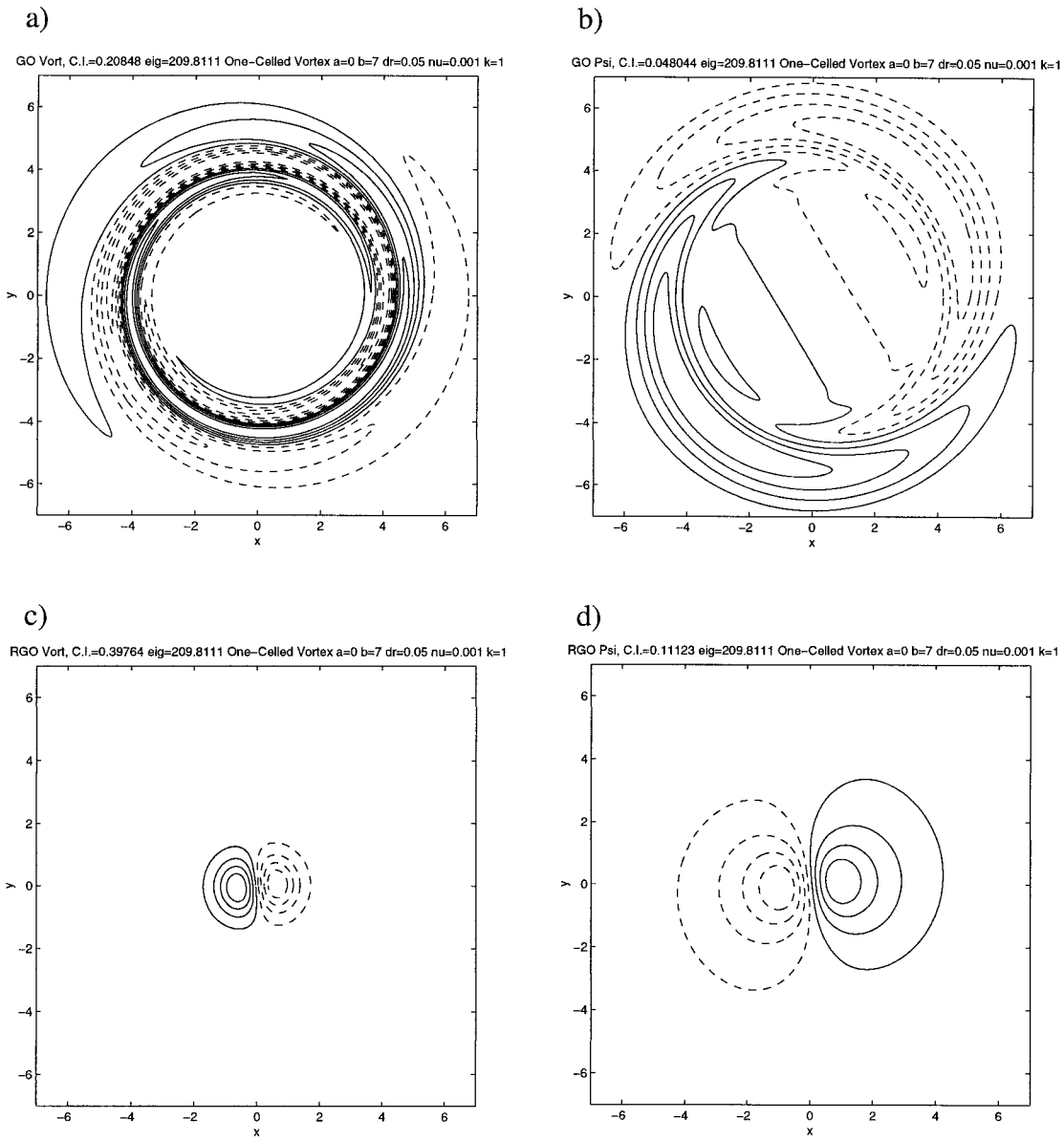

FIG. 6. The global optimal and its structure at the moment of maximum energy (realized global optimal) for $k = 1$ in the one-celled vortex: (a) GO vorticity, (b) GO streamfunction, (c) RGO vorticity, and (d) RGO streamfunction. The maximum growth in energy is indicated at the top of each plot, where the contour interval is also indicated. Negative contours are dashed.

ever, this does not directly address how these perturbations affect the mean flow itself. Just as we found the steady-state variance, we will now solve for the associated steady-state eddy momentum flux divergence and then use these eddy flux divergences to compute the tendency on the mean flow.

a. Evaluation of mean eddy momentum fluxes in a stochastically forced vortex

We would like to determine the mean eddy momentum flux divergence generated by a stochastically driven perturbation field. The eddy momentum flux divergence (equal to the local acceleration of the mean flow) at radius r is

$$\frac{\partial}{\partial t}V(r, t) = -\frac{1}{r^2}\frac{\partial}{\partial r}\overline{(r^2u'v')} = -\overline{u'(r, t)\zeta'(r, t)}$$

$$= -\frac{1}{4}[u^*(r, t)\zeta(r, t) + \zeta^*(r, t)u(r, t)]. \quad (5.1)$$

The results over the whole domain for the averaged eddy fluxes can then be written in terms of the diagonal elements of a correlation matrix:

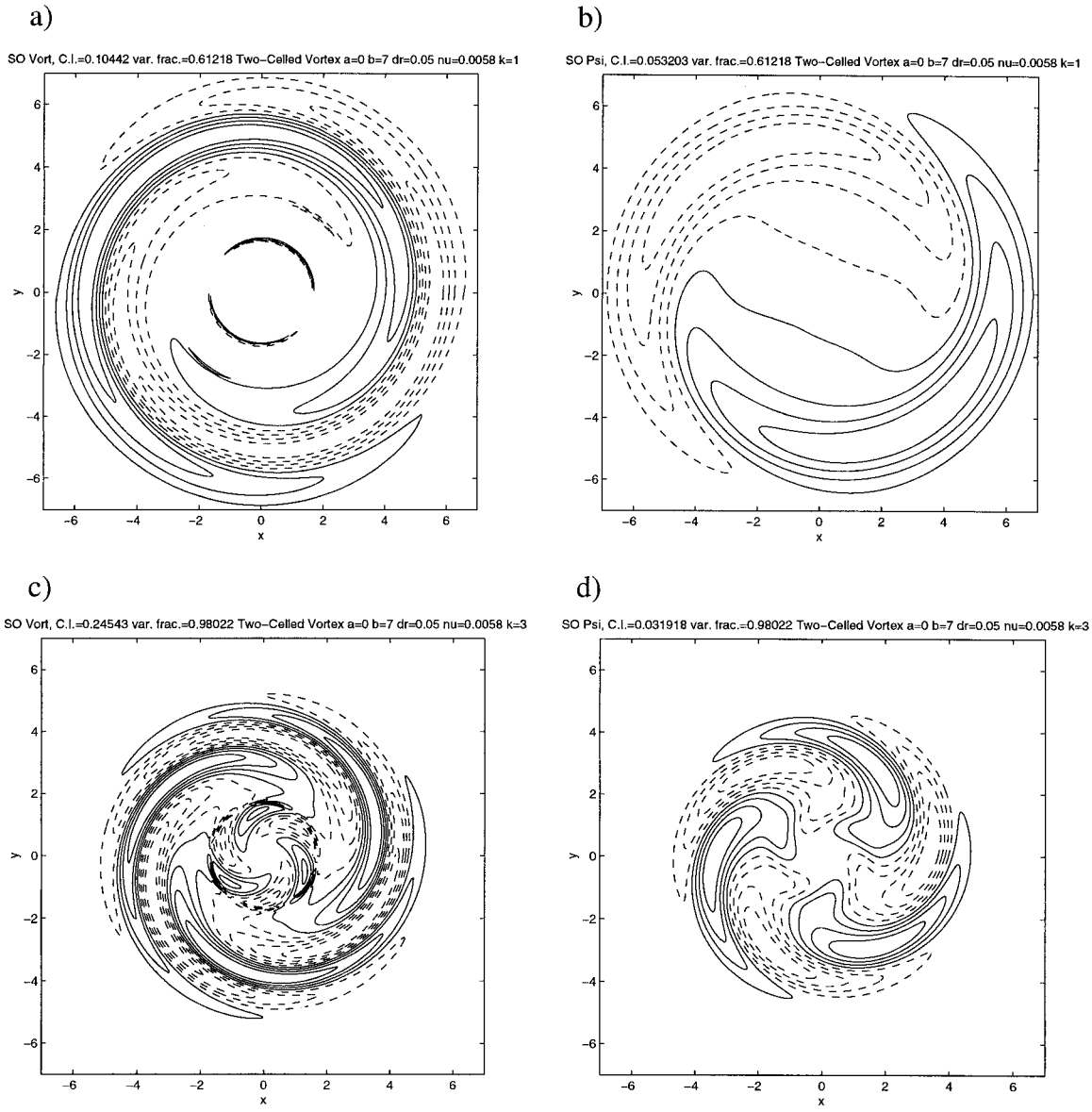

FIG. 7. Stochastic optimals (SOs) for $k = 1$ and $k = 3$ in the two-celled vortex: (a) $k = 1$ vorticity, (b) $k = 1$ streamfunction, (c) $k = 3$ vorticity, and (d) $k = 3$ streamfunction. Their fractional contribution to the variance is listed at the top of each plot, where the contour interval is also indicated. Negative contours are dashed.

$$\mathbf{Y}^t_{ij} = -\frac{1}{4}(\langle u_i(t)\zeta_j^*(t)\rangle + \langle \zeta_i(t)u_j^*(t)\rangle), \qquad (5.2)$$

where u and ζ now refer to the full vector representations of the radially varying perturbation velocity and vorticity functions for each azimuthal wavenumber.

To find the steady-state eddy fluxes, we define a correlation matrix $\mathbf{Z}^t$ for vorticity such that

$$\mathbf{Z}^t_{ij} = \langle \zeta_i(t)\zeta_j(t)\rangle. \qquad (5.3)$$

By comparison to (2.5) it is easy to see that we can solve for the steady-state vorticity correlation matrix $\mathbf{Z}^\infty$ by exactly the same procedure we used to find $\mathbf{C}^\infty$; the result will depend on the time evolution operator $\mathbf{T}$ in vorticity coordinates rather than the operator $\mathbf{A}$ in generalized velocity coordinates. Note that any second-order moment of an arbitrary correlation matrix derived from arbitrary operators $\mathbf{L}_1$, $\mathbf{L}_2$:

$$\mathbf{S}_{ij} = \langle (\mathbf{L}_1 x)_i (\mathbf{L}_2 x)_j^* \rangle \qquad (5.4)$$

can be found in terms of the operators and the correlation matrix (2.9) itself:

$$\mathbf{S} = \mathbf{L}_1 \mathbf{C} \mathbf{L}_2 \dagger. \qquad (5.5)$$

Recalling that the perturbation radial velocities can be found by operating on the vorticity with an operator based on the Green's function, we can use (5.5) to find

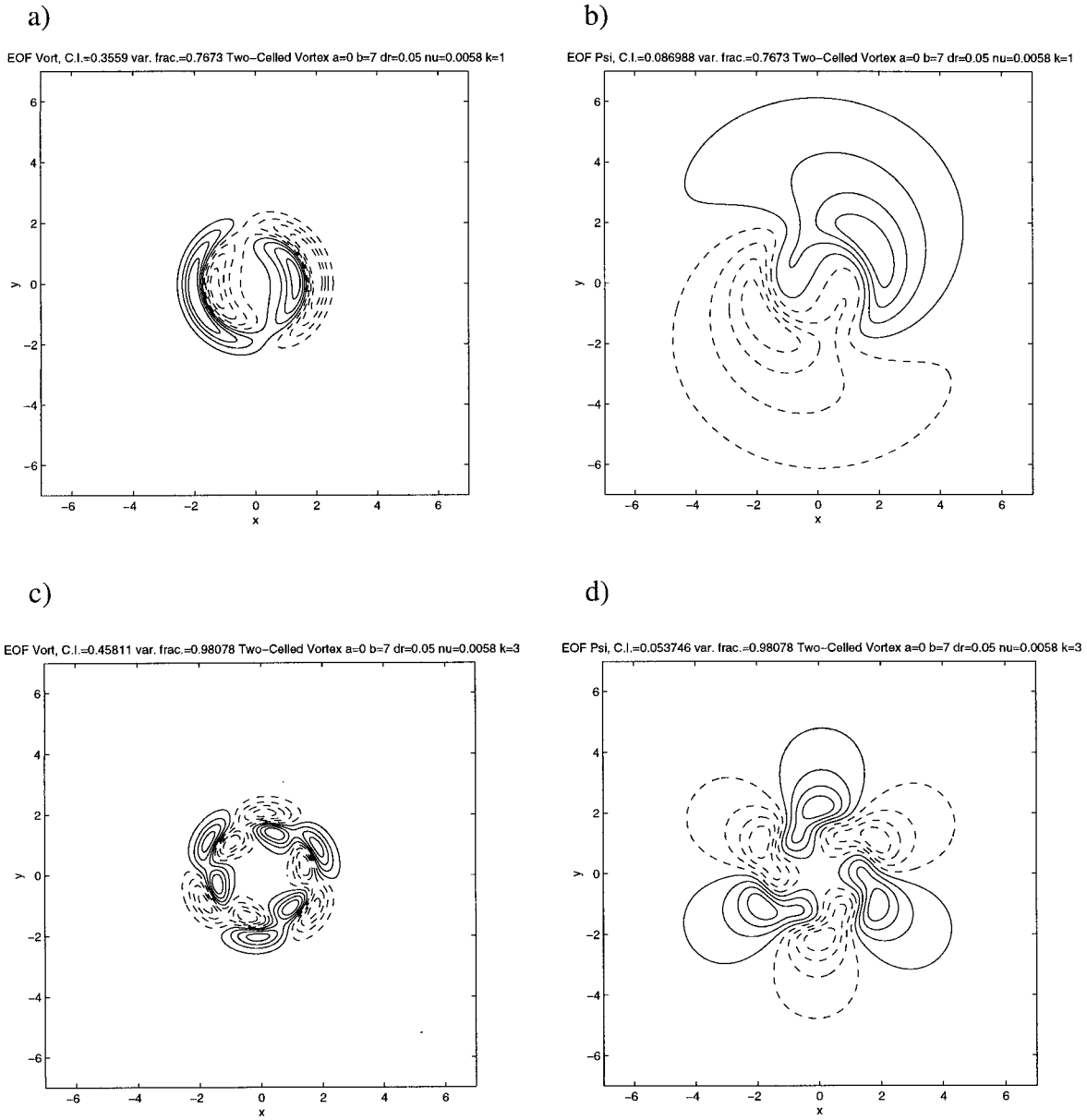

FIG. 8. EOFs for $k = 1$ and $k = 3$ in the two-celled vortex: (a) $k = 1$ vorticity, (b) $k = 1$ streamfunction, (c) $k = 3$ vorticity, and (d) $k = 3$ streamfunction. Their fractional representation of the variance is listed at the top of each plot, where the contour interval is also indicated. Negative contours are dashed.

the steady-state solution for the eddy flux divergence matrix $\mathbf{Y}^{\infty}$:

$$\mathbf{Y}^{\infty} = -\frac{1}{4}(\mathbf{U}\mathbf{Z}^{\infty} + \mathbf{Z}^{\infty}\mathbf{U}^{\dagger}), \tag{5.6}$$

where $\mathbf{U} = -ik\mathbf{R}^{-1}\mathbf{G}$ is the operator that obtains the radial perturbation velocities from the vorticity. Since the eddy flux divergence at each radius depends only on the local values of the velocity and vorticity [from (5.1)], the ensemble-averaged eddy flux divergence as a function of radius lies on the diagonal of the correlation matrix $\mathbf{Y}^{\infty}$.

b. Eddy flux divergence in the one-celled vortex

The mean eddy flux divergence for stochastically maintained perturbations in the one-celled vortex is shown in Fig. 11 for azimuthal wavenumbers $k = 1$, 2, and 16. For the lower wavenumbers we see that the net effect of the perturbations is to decelerate the flow in the vicinity of the radius of maximum winds $r = 1$, that is, on average there is a downgradient momentum flux. For all wavenumbers $k > 8$, the net effect is to accelerate the flow in the vicinity of the radius of maximum winds, as shown in this case for $k = 16$, so that there is on average an upgradient flux of momentum.

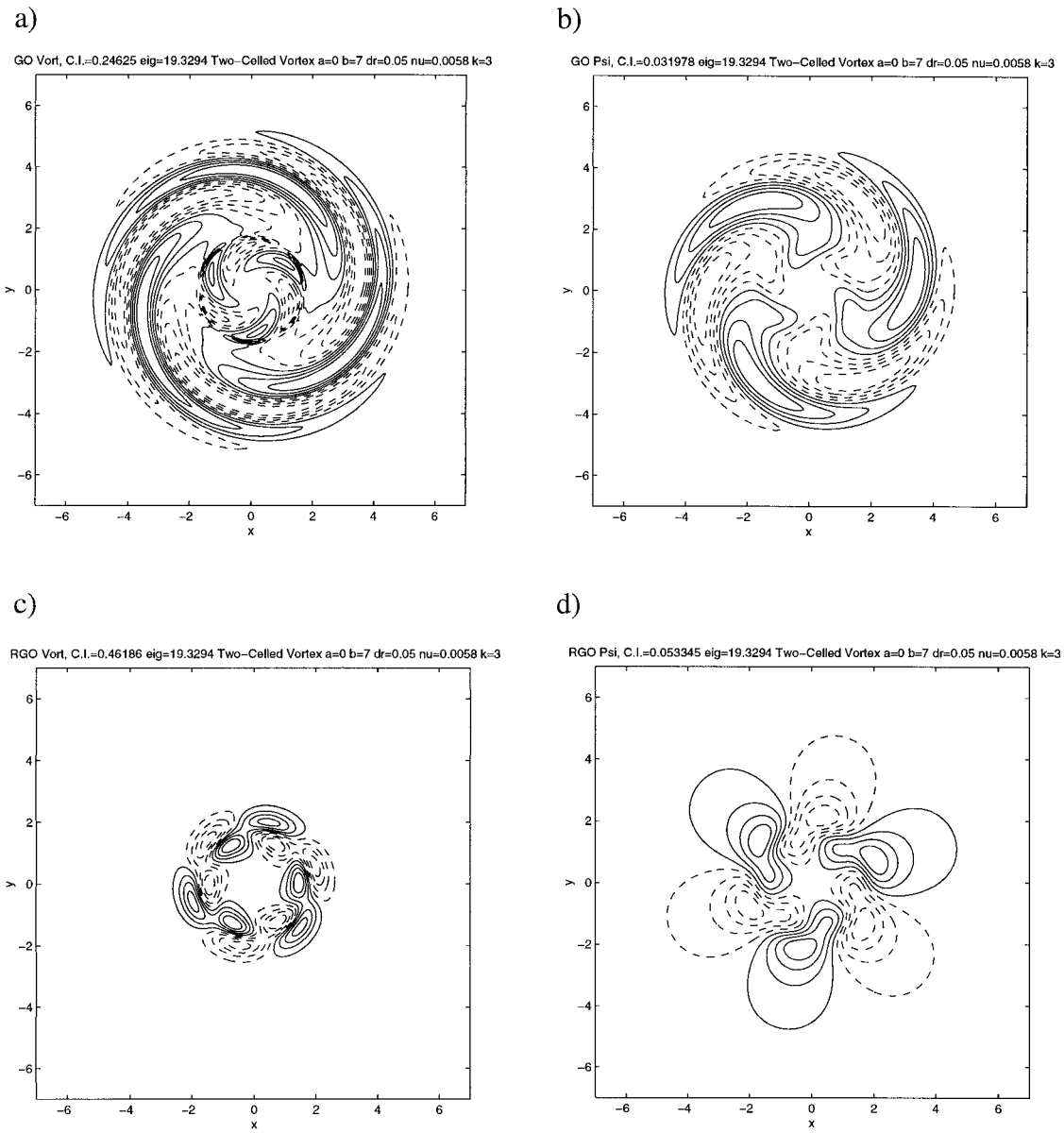

FIG. 9. The global optimal and its structure at the moment of maximum energy (realized global optimal) for $k = 3$ in the two-celled vortex: (a) GO vorticity, (b) GO streamfunction, (c) RGO vorticity, and (d) RGO streamfunction. The maximum growth is indicated at the top of each plot, where the contour interval is also indicated. Negative contours are dashed.

The reasons for this difference between the low- and high-wavenumber cases has previously been discussed to some extent by Nolan and Farrell (1999a) in the examination of the total eddy flux divergence over the lifetime of individual perturbations. It was found that whether or not the net momentum flux of a particular disturbance was upgradient or downgradient depended on the existence of nearly neutral modes at that wavenumber (i.e., the smallness of the decay rate of the eigenvalue of the least damped mode) and the extent to which these perturbations excited such modes. If these modes were indeed excited, energy acquired from the mean flow through transient growth would be trapped in the modes and not returned to the mean flow, resulting in a net downgradient momentum flux. The long-time persistence of a normal mode that is not sheared over was shown by Smith and Montgomery (1995) for the case of an inviscid, unbounded Rankine vortex. If the energy is not trapped in this manner, then most of the energy of the perturbation will eventually be returned to the mean flow, resulting in a net upgradient momentum flux. Our results here are therefore a generalization of our previous results to the case where all perturbations are excited equally.

c. Eddy flux divergence in the two-celled vortex

The mean eddy flux divergence under stochastic forcing in the two-celled vortex is shown in Fig. 12 for wavenumbers $k = 1$, $k = 4$, and $k = 8$. The results for all three wavenumbers in this case are similar to the low-wavenumber results above in that the flow is being decelerated in the vicinity of the RMW at $r = 2.19$. However, the flow is being accelerated *inside* the radius of maximum winds, so that the mean momentum flux is inward rather than outward (but still downgradient). This result is similar to what was found by Lewellen et al. (1997) in their three-dimensional numerical simulations of a tornado vortex, and also by Rotunno (1978) in his study of the instabilty of cylindrical vortex sheets: the effect of the multiple vortices on the surrounding flow was to transport angular momentum *inward.* The result for $k = 8$ is different from the lower wavenumbers in two ways: 1) the local accelerations are orders of magnitude smaller, and 2) there is a substantial positive acceleration just outside the large negative acceleration in the vicinity of RMW. Thus for higher wavenumbers we find that momentum is fluxed both outward and inward from the radius of maximum winds.

d. Resulting mean flow deviations

The two preceeding sections have shown us the ensemble-average acceleration to the mean vortex flow caused by a stochastically maintained perturbation field. However, this does not directly tell us what we really want to know, which is the change in the mean vortex flow resulting from these accelerations. This is because the mean vortex flow is experiencing the same advection due to the radial inflow and dissipation as are the perturbations, as presented in (3.3). Positive or negative perturbations to the symmetric azimuthal velocity function will be both advected into the core and smoothed by diffusion. Let us write the total perturbed symmetric flow as

$$V(r, t) = \overline{V} + V'(r, t), \tag{5.7}$$

where $\overline{V}$ is the steady-state solution to (3.3) and V' is its deviation. Substituting (5.7) into (3.3), and including the effects of the eddy flux divergences of the stochastically maintained perturbations, we have an equation for the evolution of the *symmetric* perturbations:

$$\frac{\partial}{\partial t}V' + U\frac{\partial}{\partial r}V' + \frac{UV'}{r} = \nu\left(\frac{\partial^2}{\partial r^2}V' + \frac{1}{r}\frac{\partial}{\partial r}V' - \frac{V'}{r^2}\right) - \sum_{k=1}^{n}\overline{u_k\zeta_k}, \tag{5.8}$$

where the summation is over all the wavenumbers under consideration. In this report we consider only one wavenumber at a time. Once the ensemble average eddy flux divergence has been found from (5.6), we may solve for the ensemble-average solution for the mean flow deviation in a manner similar to the solution of (3.3) [see Nolan and Farrell (1999a)] by setting the time rate of change of V' to zero.

Figure 13 shows the ensemble-average mean flow deviation caused by stochastically maintained perturbations for $k = 1$ and $k = 2$ in the one-celled vortex. For $k = 1$, we see that the mean flow is increased for $r > 1$ and decreased for $r < 1$. This is somewhat surprising since the local effect of the perturbations is to decelerate the flow at $r = 1$, as shown in Fig. 11a. However, a closer examination of Fig. 11a shows a small positive acceleration of the mean flow much farther outside the core of the vortex—in the vicinity of $r = 6$. This positive anomaly is advected into the vortex core and amplified by conservation of angular momentum. Thus the effect of this small positive acceleration at large radius is to cause a substantial positive mean flow deviation at $r = 2$ and to almost completely eliminate the effects of the large negative acceleration in the vortex core. For $k = 2$, the effect of positive accelerations at a larger radius (see Fig. 11b) is even more pronounced, such that the average mean flow deviation is positive everywhere with a maximum near $r = 1.2$, that is, very close to the radius of maximum winds. Results for all higher wavenumbers were similar.

The fact that the change in the azimuthal velocity field can be positive everywhere might seem paradoxical. Since the forcing functions are asymmetric, the instantaneous angular momentum input at any moment must be zero. In fact for all our calculations we found that the statement

$$\int_0^b \langle -\overline{u'\zeta'}\rangle r^2\, dr = 0 \tag{5.9}$$

was true to within machine accuracy. How then can forcing with zero net torque result in a nonzero change in the angular momentum of the vortex? Recall that the fluid parcels in the vortex are being advected inward by the mean radial inflow, which also varies as a function of radius. The parcels move inward slowly when $-U(r)$ is small and quickly where $-U(r)$ is large. Thus, *the total angular momentum imparted to the parcels depends how long they spend in the regions of positive or negative eddy flux divergence.* In the case just shown for the one-celled vortex with $k = 2$, we saw a small positive acceleration on the mean flow in the vicinity of $r = 5$ (see Fig. 11b). Referring to the radial velocity profile in Fig. 1a, we see that $-U(r)$ is indeed very small in the same place, so a large amount of positive angular momentum is acquired by the mean flow in this location. Note also one of the peaks in the negative acceleration is in a place where the radial velocity is relatively high, again contributing to the net positive change.

This may still seem inconsistent with angular momentum conservation since the total change in angular momentum of the mean flow is positive, while the net

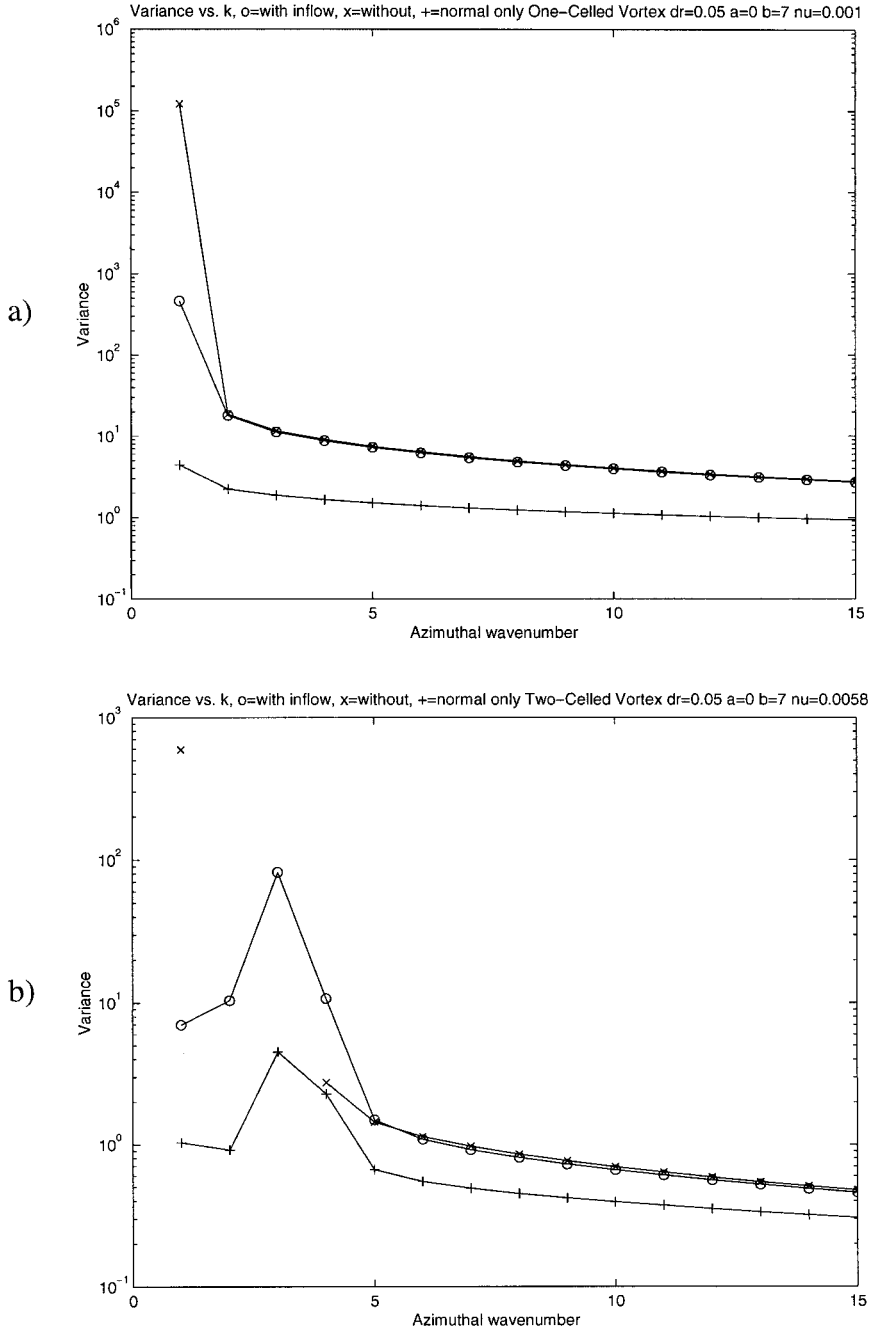

FIG. 10. Sustained variance in (a) the one-celled vortex and (b) the two-celled vortex under stochastic forcing as a function of azimuthal wavenumber; ○'s: the standard variance; ×'s: the same variance with the radial inflow effects neglected; +'s: the equivalent normal variance of the vortices with inflow. The variance without inflow is not shown for $k = 2$ and $k = 3$ in the two-celled vortex because the vortex is unstable without inflow for these wavenumbers.

torque of the forcing is zero. However, these swirling flows sustained by radial inflow are not in fact closed systems but are supplied with angular momentum by the outer boundary conditions. This source is meant to be representative of the larger supply of rotating fluid that exists in the storm environment. The azimuthal velocity profiles for the one- and two-celled vortices are the results of a balance between advection and diffusion of angular momentum. When we add the eddy flux divergence caused by the stochastically forced eddies, a new balance is achieved that may have a different total amount of angular momentum than the original vortex.

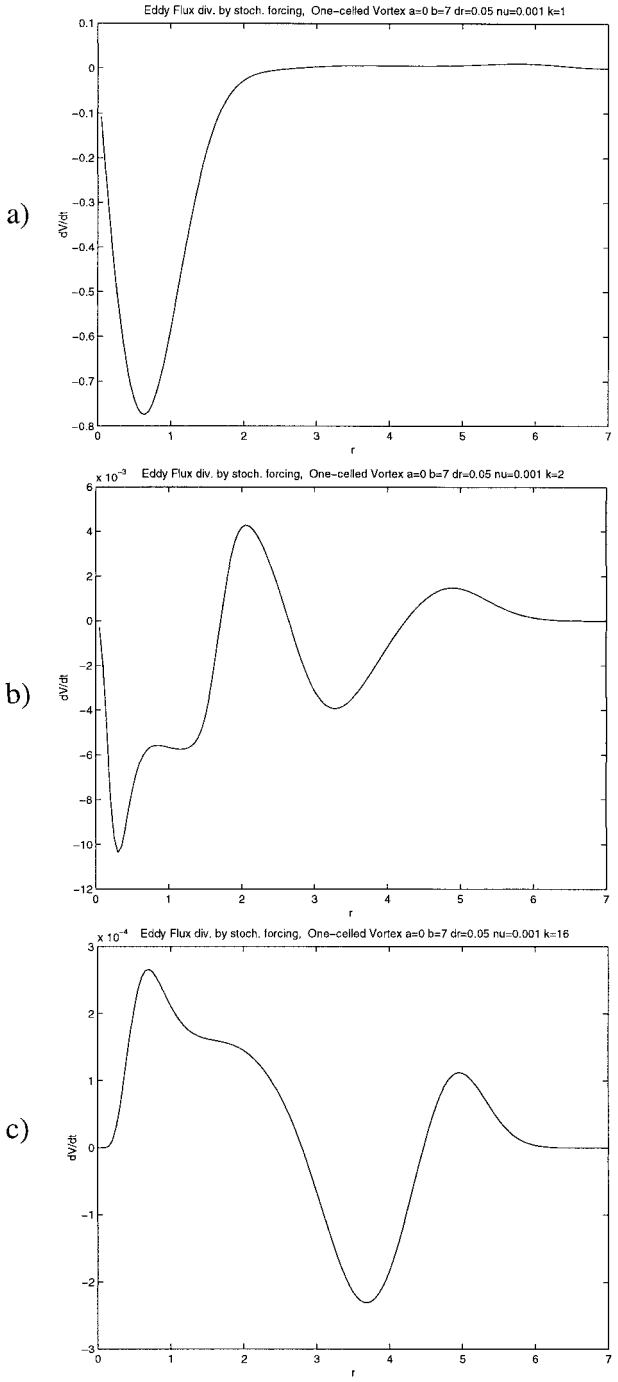

FIG. 11. Ensemble-average eddy flux divergence caused by perturbations sustained by stochastic forcing in the one-celled vortex for (a) $k = 1$, (b) $k = 2$, and (c) $k = 16$.

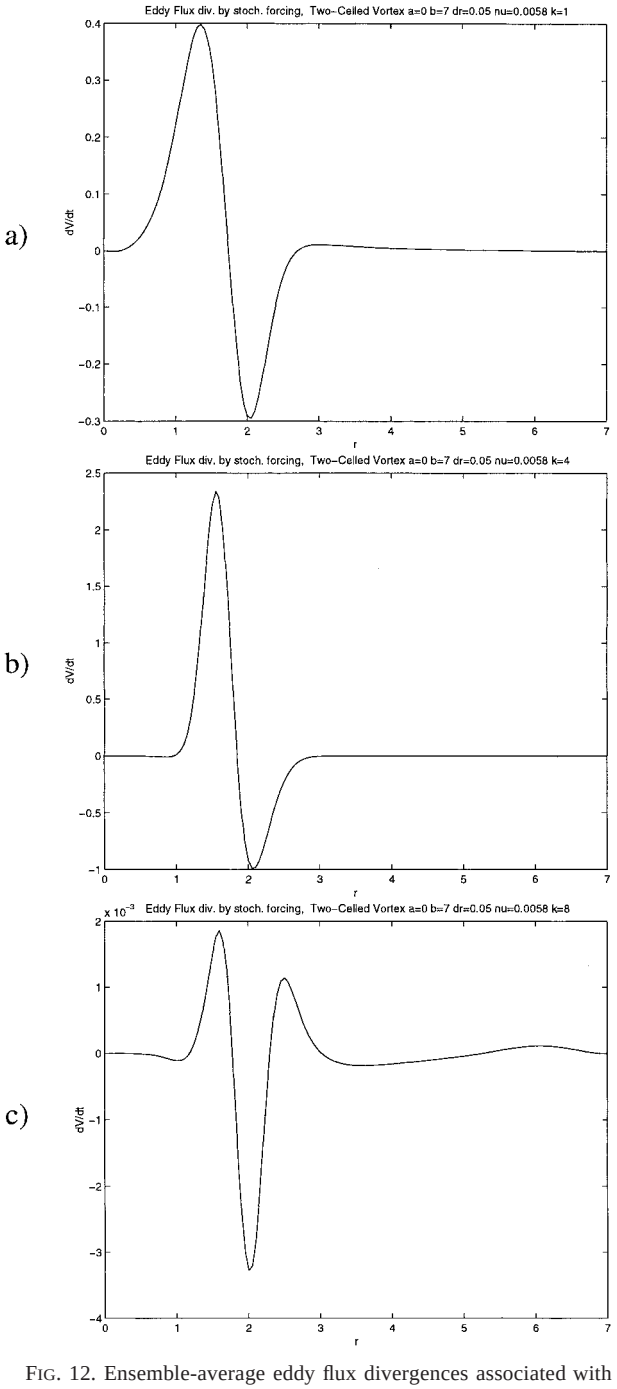

FIG. 12. Ensemble-average eddy flux divergences associated with the stochastically maintained perturbations in the two-celled vortex for (a) $k = 1$, (b) $k = 4$, and (c) $k = 8$.

We must also recognize that the change in the mean flow is highly dependent on the structure of the radial inflow, a fact that we must consider carefully if we try to apply the knowledge learned here to realistic geophysical vortices.

Radial inflow has a substantial impact on how stochastically maintained perturbations ultimately affect the mean flow. To emphasize this point, we have recalculated the mean eddy flux divergences and the resultant average mean flow deviations in an identical one-celled vortex with the radial inflow eliminated. The results, shown in Fig. 14, are strikingly different from before. First, the predicted accelerations and mean flow

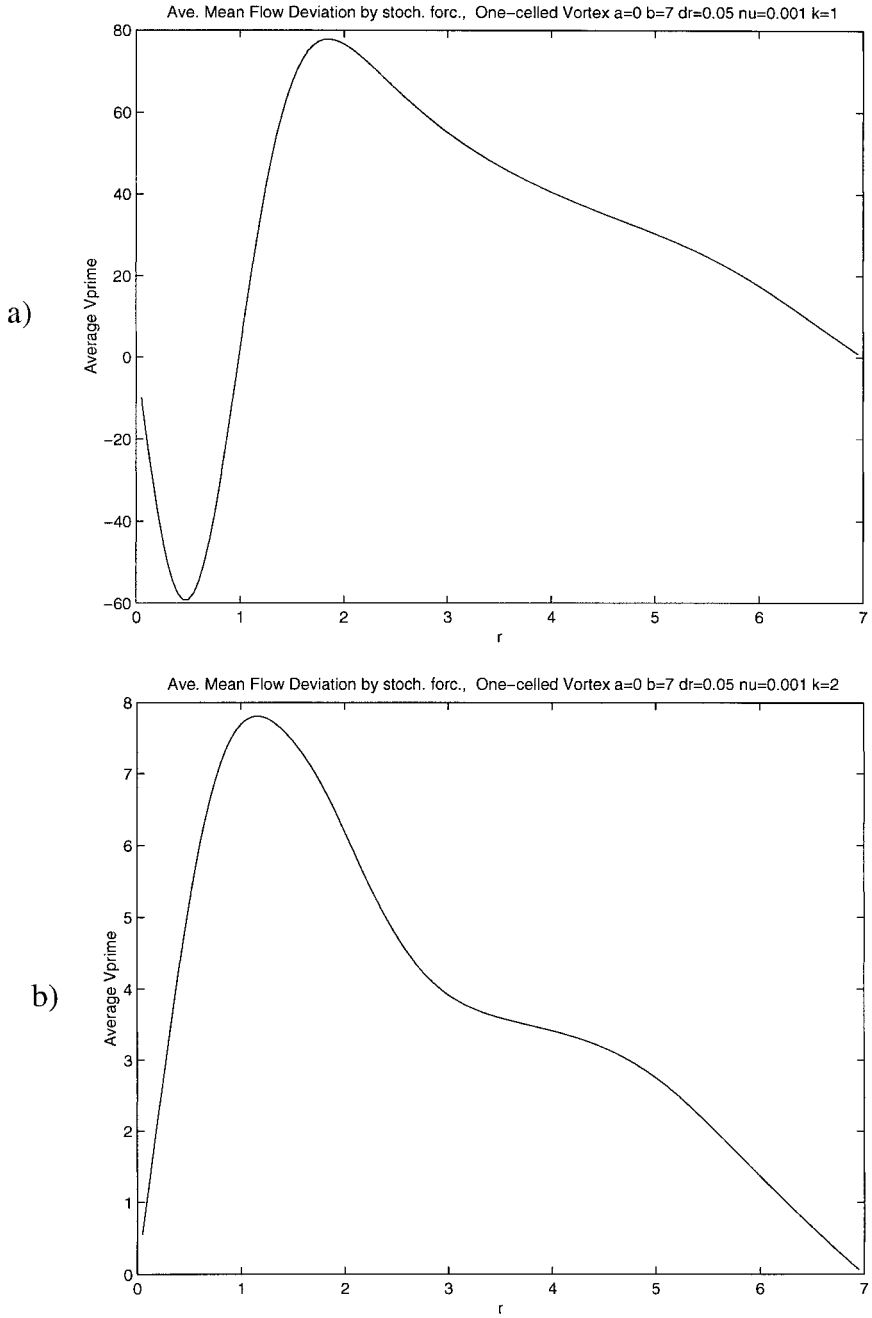

FIG. 13. The resulting average mean flow deviations caused by the stochastically maintained eddy flux divergence in the one-celled vortex: (a) $k = 1$ and (b) $k = 2$.

changes are orders of magnitude larger than when the inflow was included. Second, we see that the ultimate effect of the perturbations for both $k = 1$ and $k = 2$ is to decrease the maximum wind speed and to increase the radius of maximum winds, that is, to make the vortex broader and less intense.

The average mean flow deviations for $k = 1$ and $k = 8$ in the two-celled vortex are shown in Fig. 15 (where the effects of radial inflow have again been included). We see that for $k = 1$, the mean flow deviation is negative near the radius of maximum winds at $r = 2.19$ and positive inside the vortex core. This result is similar to what one might expect from examination of the average eddy flux divergence previously shown in Fig. 12a. For $k = 8$, however, we see that the average change in the mean flow is positive for all r, for the same reasons described above for $k = 2$ in the one-celled vortex.

The eddy momentum fluxes and resulting average

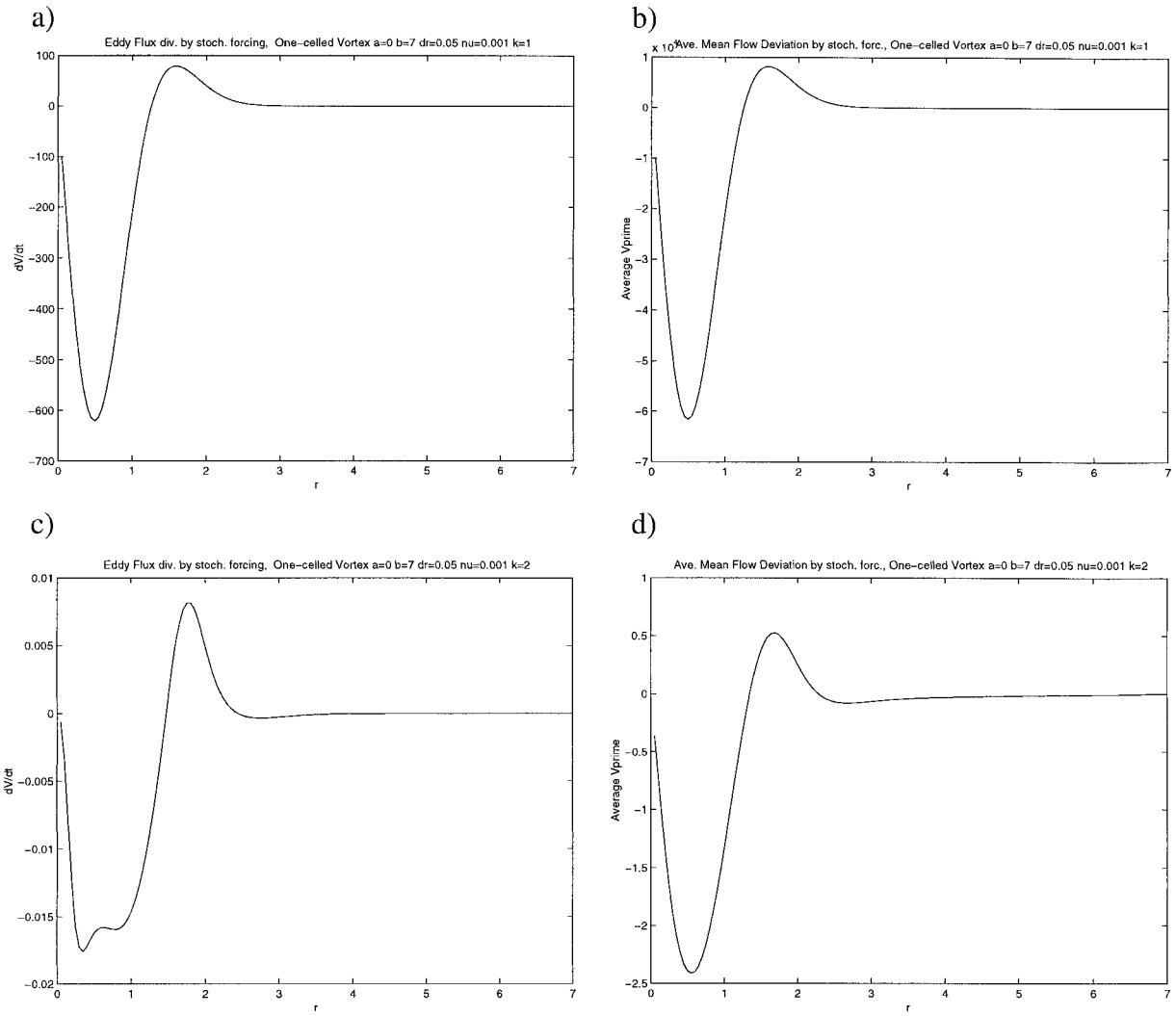

FIG. 14. The average eddy flux diverences and resultant mean flow deviations in the one-celled vortex, recomputed with the radial inflow eliminated: (a) average eddy flux diveregnce, $k = 1$; (b) average mean flow deviation, $k = 1$; (c) average eddy flux divergence, $k = 2$; (d) average mean flow deviation, $k = 2$.

mean flow deviations in the two-celled vortex recalculated without radial inflow are shown in Fig. 16. The results here are analogous to those for the one-celled vortex without radial inflow: for the lower, nearly unstable wavenumber $k = 1$, the eddy flux divergences and mean flow deviations are orders of magnitude larger; for $k = 8$, the formerly everywhere positive mean flow deviations are negative in the vicinity of RMW.

6. Discussion

a. The least damped mode as a determining factor in the stochastic dynamics

While a variety of linear perturbation dynamics have been observed in the preceding sections, the results of stochastic forcing of our two vortex types can generally be separated into two cases.

In case I the stochastic forcing excites transient growth of initially upshear-tilted perturbations, which are sheared over by the mean flow, reach their maximum energy when they have evolved into a compact structure, then are sheared over further and give their energy back to the mean flow. While a small amount of energy is lost to dissipation along the way, almost all the initial disturbance energy and the energy acquired from the mean flow during the growth phase are returned to the mean flow through upgradient eddy momentum fluxes. In this case the input energy of the stochastic forcing ends up in the mean flow and the vortex is intensified. This vortex intensification is the long-time mean effect of the continuous axisymmetrization of the stochastically driven asymmetries, similar to the axisymmetrization of particular asymmetric initial conditions demonstrated with linear calculations by Smith and Mont-

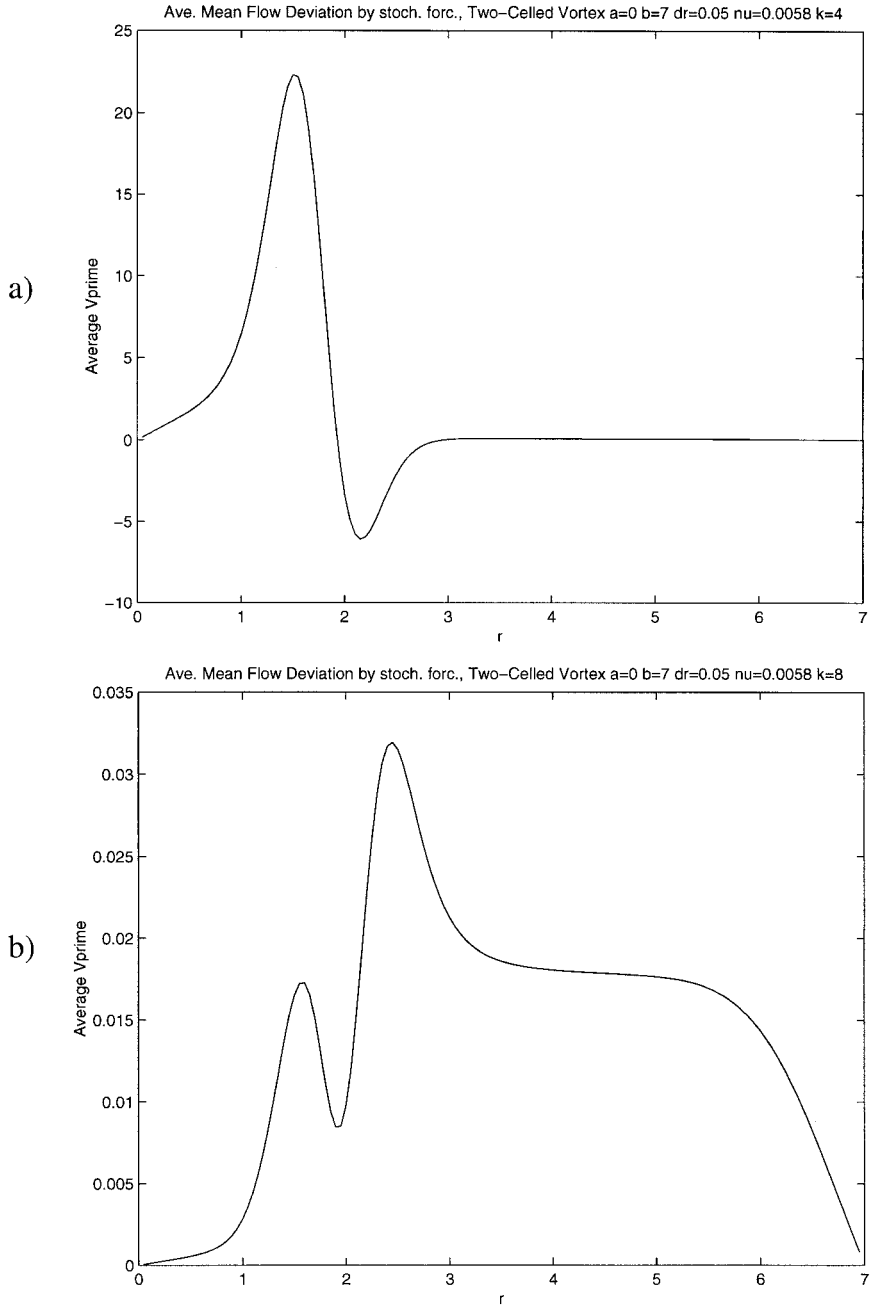

FIG. 15. The average mean flow deviations in the two-celled vortex caused by the stochastically maintained perturbations: (a) $k = 4$ and (b) $k = 8$.

gomery (1995) and in fully nonlinear computations by Melander et al. (1987).

In case II the stochastic forcing again excites transient growth; however, in this case the decay rate of the least damped mode is extremely small [e.g., the least damped mode decay rate is 2.1×10^{-3} for $k = 1$ in the one-celled vortex (equivalent to a decay timescale of 7.9 min in a tornado) and 9.3×10^{-4} for $k = 3$ in the two-celled vortex (a decay timescale of 29.3 h in a hurricane)], and these modes are also similar to the coherent structures that the transiently growing disturbances become when they reach their maximum energy. The transiently growing disturbances then project strongly onto the least damped modes and their energy is trapped there; in other words, the least damped modes interact with the mean flow vorticity gradient so that they sustain themselves and are not sheared over by the mean flow. In this case, disturbance energy ''accumulates'' in the nearly neutral modes and the energy is not returned to the mean flow but is instead lost through dissipation

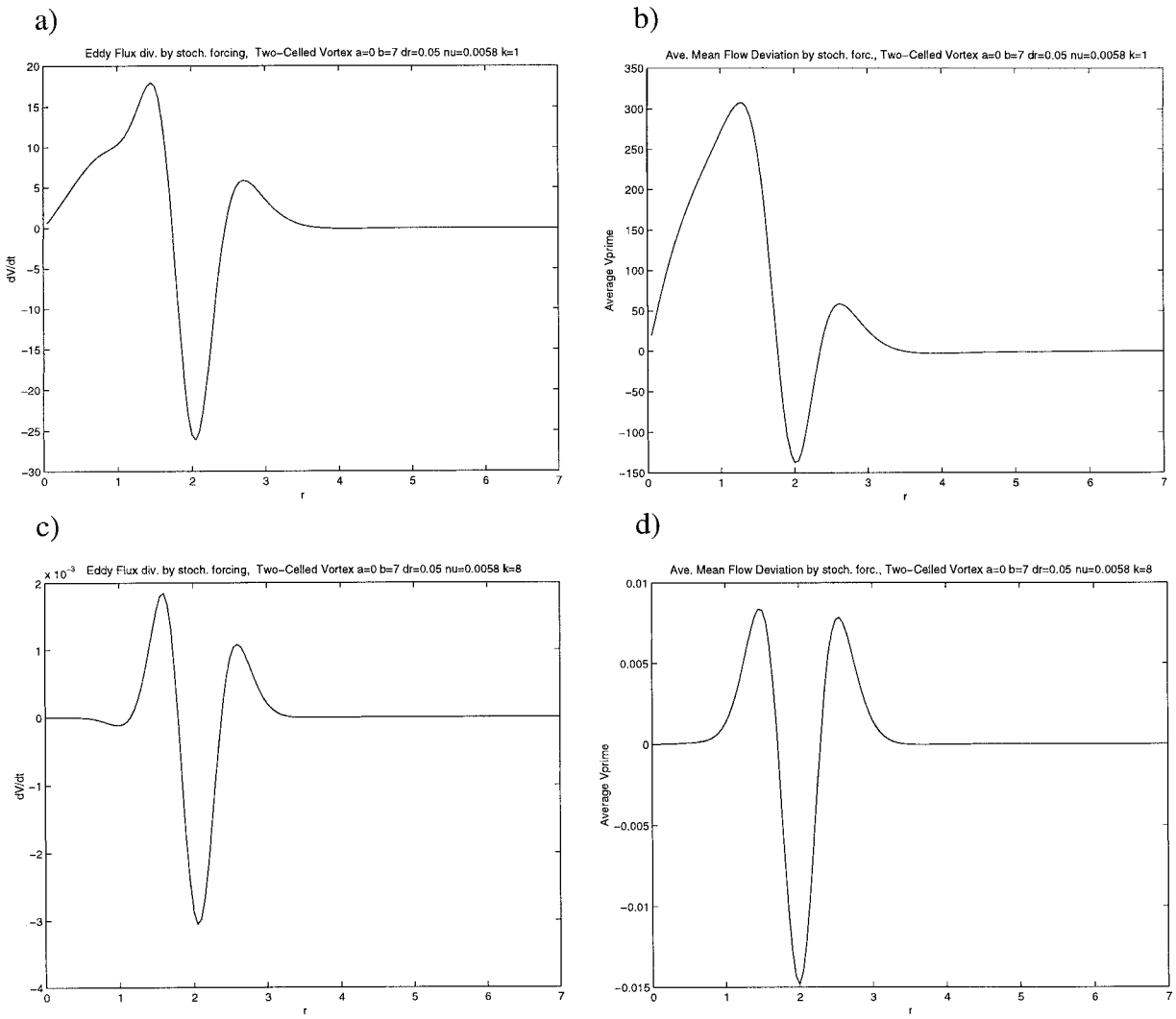

FIG. 16. The average eddy flux diverences and resultant mean flow deviations in the two-celled vortex, recomputed with the radial inflow eliminated: (a) average eddy flux diveregnce, $k = 4$; (b) average mean flow deviation, $k = 4$; (c) average eddy flux divergence, $k = 8$; and (d) average mean flow deviation, $k = 8$.

very slowly over long times. Since the disturbances are never sheared over to cause upgradient momentum fluxes, only downgradient momentum fluxes occur and the vortex is weakened.

In case II, the sustained variance can be orders of magnitude larger than in case I. Comparing these two cases we understand why for some wavenumbers radial inflow has a significant effect on the results: including the effects of radial inflow has the stabilizing effect of increasing the decay rates of the least damped modes for the cases of $k = 1$ in the one-celled vortex and $k = 1$, $k = 2$, and $k = 3$ for the two-celled vortex.

b. *Comparisons with recent results regarding tropical cyclones*

As mentioned in the introduction, asymmetric disturbances have received considerable attention in connection with tropical cyclone dynamics, with much of the emphasis on how these disturbances affect the tropical cyclone track and on their relationship to spiral bands. However, asymmetric dynamics have also been considered as a mechanism for hurricane intensification, originally by Pfeffer (1958) and more recently by Challa and Pfeffer (1980), Pfeffer and Challa (1981), Carr and Williams (1989), Montgomery and Kallenbach (1997), and Montgomery and Enaganio (1998). In this last report the authors used a three-dimensional quasigeostrophic model to demonstrate how coherent potential vorticity anomalies, injected in bursts so as to model episodic convection, are sheared over by the larger-scale vortex flow and ultimately cause upgradient momentum fluxes.

While the works cited above have focused specifically on tropical cyclones, the previous studies by Nolan (1996), Nolan and Farrell (1999a), and this report have

attempted to illustrate the phenomena of axisymmetrization and asymmetric vortex intensification in a more idealized class of vortices sustained by convergence and also to a wider class of asymmetric forcings. One major distinction between our work and most of the studies cited in the introduction and above [except Carr and Williams (1989)] is that both our mean vortex flows transition rapidly to a potential ($1/r$) vortex just beyond of the radius of maximum winds. A potential flow has no vorticity, so there is no mechanism for the propagation of waves away from the vortex. The azimuthal wind fields of hurricanes generally have a slower decay with radius, perhaps more like $r^{-1/2}$, which allows for the existence of waves on an associated mean vorticity gradient. Such waves, sometimes called ''vortex–Rossby waves'' were examined by Montgomery and Kallenbach (1997), who explained their dynamics and showed how downshear tilted disturbances always propagate away from the core of the vortex. The outward propagation of spiral bands has in fact been demonstrated with analyses of radar observations of hurricanes by Gall et al. (1998). In our vortices there are no such waves in the potential flow region and the phenomenon of momentum and energy transport away from the vortex by vortex–Rossby waves does not occur.

Does the outward propagation of energy and momentum by vortex–Rossby waves play a significant role in the redistribution of momentum under stochastic forcing? To address this possibility we applied our method of analysis to a vortex with a more substantial vorticity gradient beyond the RWM. An example of such a velocity profile would be

$$V(r) = \frac{1.5r}{0.5 + r^{1.5}}. \tag{6.1}$$

This velocity profile is based on the one used by Montgomery and Kallenbach (1997) except that is has been modified so that it transitions from solid-body rotation in the core to an $r^{-1/2}$ velocity profile in the far field. This velocity profile and its vorticity gradient, which for large r goes like $r^{-5/2}$, are shown in Fig. 17. To increase the detail in our calculations, we reduce the outer radius to $b = 5$ and change the grid size to $\Delta r = 0.02$. We set $\nu = 0.0001$. The mean radial velocity $U(r) = 0$.

The resulting EOFs and eddy flux divergences under unitary stochastic forcing for the $r^{-1/2}$ vortex were very similar to all the results for our previous one-celled vortex without radial inflow. The response for $k = 1$ is always dominated by the pseudomode, regardless of the structure of the forcing functions. However, for higher wavenumbers we can observe a response that indicates the existence of vortex–Rossby waves if we restrict forcing matrix $\mathbf{F}$ to a single coherent vorticity anomaly centered at the RMW, of the form:

$$F(r) = e^{-(r-1.02)^2/0.4}, \tag{6.2}$$

such that the vorticity forcing is effectively zero everywhere except for $0.5 < r < 1.5$. Similar disturbances have been used previously as a simple model of the effects of convection near the eyewall (Carr and Williams 1989; Montgomery and Kallenbach 1997; Montgomery and Enaganio 1998).

The primary EOF that arises from this convective-type stochastic forcing, which represents 90.5% of the variance, is quite different than what we have seen before. Note that the sizes of the axes in Fig. 18a have been decreased so that the small-scale structure of the EOF can be seen more clearly. The primary EOF shows downshear spirals emanating from the region of vorticity input. This outer structure is very much like the vortex–Rossby waves analyzed by Montgomery and Kallenbach (1997). The complex magnitude of the primary EOF vorticity as a function of radius is shown in Fig. 18b. Note that the peak in the vorticity response is at a slightly larger radius than the peak of the vorticity forcing function, and that the support of the EOF vorticity extends farther out than the forcing function, which is effectively zero for $r > 1.5$. Calculations with smaller values of the viscosity (not shown) demonstrated that this outward extension of the vorticity was not caused by diffusion. However, if there is indeed transport of angular momentum and energy by outward-traveling waves, they are not being carried much further than 50% beyond the radius of maximum winds. This is indicated by the eddy momentum flux divergence, which shows a substantial acceleration of the mean flow just inside $r = 1$ with smaller decelerations on either side of this peak. For $r > 2$, however, the mean flow is essentially unaffected. Results for higher wavenumbers were similar, with the region affected by the outward spirals being even more limited. This is consistent with the analysis of Montgomery and Kallenbach (1997), which showed that the outward propagation of Rossby waves decreases rapidly with wavenumber.

Let us rescale the eddy flux divergences shown in Fig. 18c to dimensional values for a hurricane with an RMW of 20 km and a $V_{\max}$ of 40 m s^{-1}. The energy input from the stochastic forcing has been normalized to be equal to one unit of energy per unit time. It would be very difficult to guess what the correct energy input rate would be for wavenumber $k = 2$ anomalies forced by convection in an actual hurricane. However, since we know the $k = 2$ *response* for a given energy input, we can modify the input such that the response (EOF) vorticity is a reasonable fraction of the mean flow vorticity. Analyses of hurricane wind fields indicate that at their maximum, wavenumber 2 anomalies are on the order of 20% of the local mean flow vorticity (Reasor and Marks 1999). The vorticity magnitude shown in Fig. 18c, with a maximum of 11.83, has been renormalized so that it has the correct energy, given the fractional response of the total energy (variance), which the primary EOF represents. However, the vorticity of the mean flow (6.1) is equal to 1.0 at $r = 1.0$. Thus, we must rescale the forcing functions in $\mathbf{F}$ so that the max-

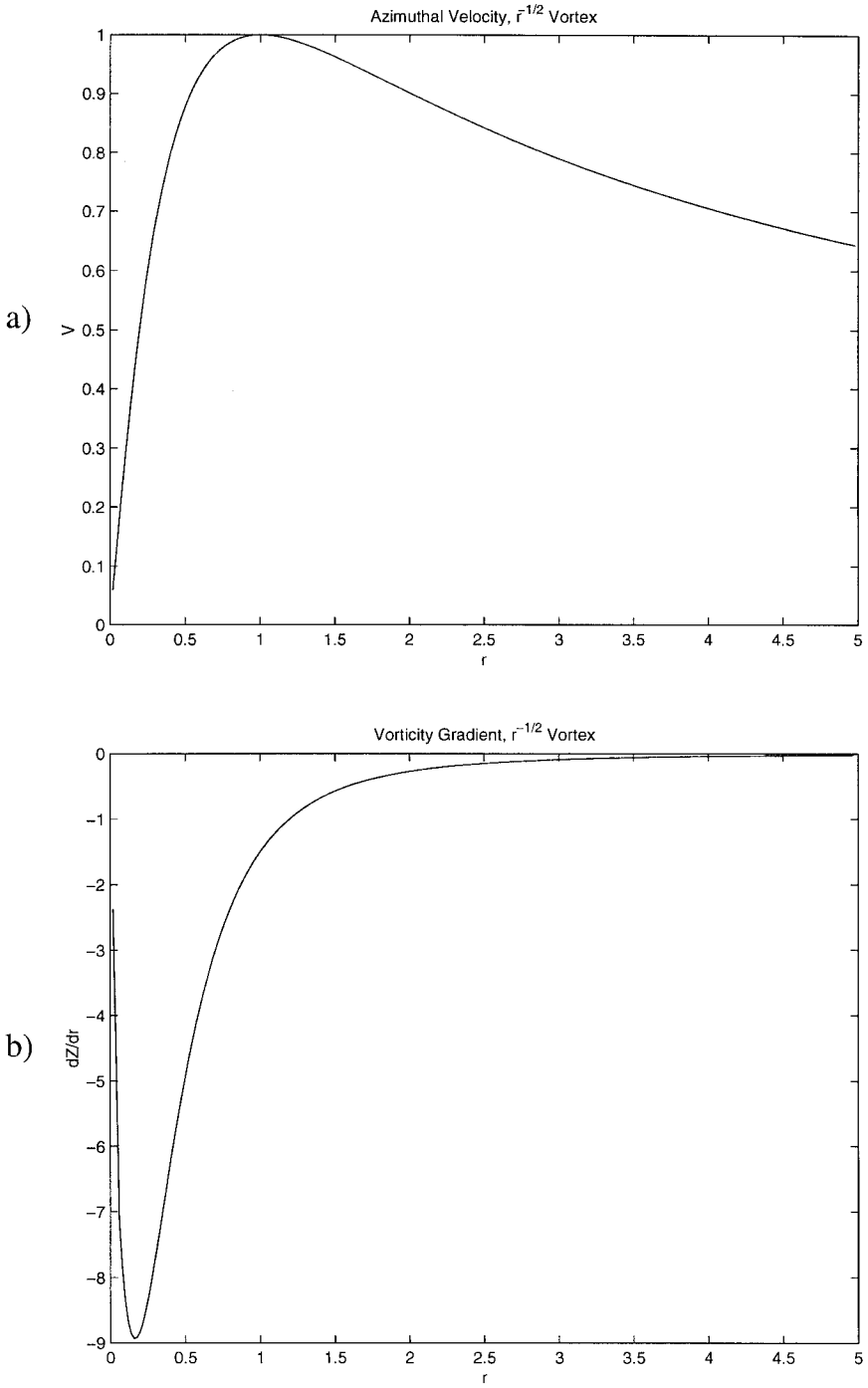

FIG. 17. (a) Velocity profile and (b) vorticity gradient for the $r^{-1/2}$ vortex.

imum vorticty response is equal to 0.2. Upon doing so, the maximum eddy flux divergence is decreased from 3.8 to 1.1 $\times$ 10^{-3}. Appropriate dimensional scales are $L = 20$ km, $U = 40$ m s^{-1}, and $T = 500$ s. Using these dimensional scales, we find the stochastic forcing causes a maximum acceleration on the hurricane wind field of 7.3 m s^{-1} day^{-1}.

Along with the fact that the vorticity is localized around $r = 1$, the ''convective'' forcing case is fundamentally different from unitary forcing in that the perturbations are radially aligned, that is, they are initially tilted neither upshear or downshear. Since they are immediately sheared over by the mean flow, their momentum fluxes are always upgradient and the relative excitation of the normal-mode type structures is substantially decreased. We should append our conclusions

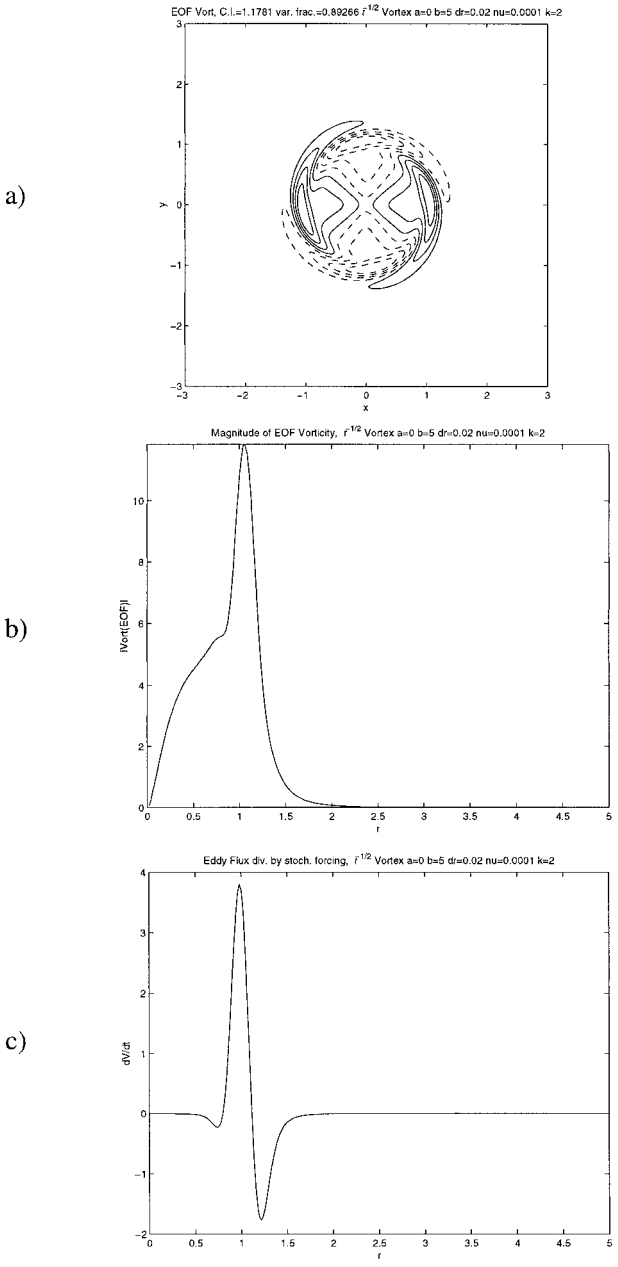

FIG. 18. Response of the $r^{-1/2}$ vortex under ''convective'' stochastic forcing for $k = 2$: (a) primary EOF, (b) complex magnitude of the primary EOF, and (c) mean eddy flux divergence.

in the previous section to say that whether or not there is net upgradient or downgradient momentum fluxes depends both on the availability of nearly neutral modes *and* the extent to which the forcing projects onto the stochastic optimals.

7. Conclusions

In this report we have extended the earlier analysis of Nolan and Farrell (1999a) to examine the response of a vortex with radial inflow to random forcing by asymmetric disturbances. The results have shown that under such forcing that is unbiased in space and time, the previously identified global optimals play a dominant role in the transfer of energy from the mean flow to the perturbations. For stable wavenumbers where nearly neutral (i.e., almost unstable) modes are present, the variance excited by the stochastic forcing and amplified by wave–mean flow interactions can be very large. This variance is greatly overestimated if the effects of the radial inflow that sustains the mean flow are neglected in the dynamics of the perturbations.

For all but the lowest wavenumbers in both one- and two-celled vortices, the net effect of the momentum fluxes associated with the stochastically maintained eddies is to intensify the vortex, that is, to increase the maximum wind speed. We also note the important observation that this effect is enhanced by the presence of the radial inflow, and that neglecting the dynamical effects of the radial inflow in these vortices produces quite opposite results in some cases. Thus we have shown that even when there is continuous excitation of perturbations that are favorably configured for transient growth (and therefore cause downgradient momentum flux), the radial inflow that sustains the mean vortex will help to ensure that the net effect of these disturbances will be to intensify the vortex.

The two-dimensional vortices with radial inflow that we have constructed are certainly crude models of intense atmospheric vortices, and our analysis neglects all three-dimensional dynamics, which of course may be important. We have, however, shown how disturbances, which are either generated within the vortex itself (such as mesoscale bursts of convection in tropical cyclones), or are carried into the vortex core by the convergent radial inflow (such as turbulent eddies in the surrounding environment of a tornado), can contribute to the intensification and maintenance of these vortices by causing upgradient momentum fluxes and transferring their kinetic energy to the mean flow. In the future, we hope to determine the robustness of this mechanism as the symmetric flow is allowed to change according to the eddy momentum fluxes, perhaps with a quasi-linear adjustment of the mean flow or with fully nonlinear simulations.

Acknowledgments. The authors would like to thank M. Montgomery for many helpful comments and advice on hurricane dynamics, and P. Ioannou and T. DelSole for many helpful discussions. We would also especially like to thank D. Adalsteinsson for helping us to make tremendous improvements in the production and appearance of our contour plots. Preliminary work for this report was prepared as part of the Ph.D. thesis of D. Nolan while he was a student at Harvard University, during which he was supported by NSF Grants ATM-9216813 and 9623539; since November of 1996 D. Nolan has been supported by the Applied Mathematical

Sciences Subprogram of the Office of Energy Research, U.S. Department of Energy under Contract DE-AC03-76SF-00098. B. Farrell was supported by NSF Grants ATM-9216813 and 9623539.

REFERENCES

Burgers, J. M., 1948: A mathematical model illustrating the theory of turbulence. *Adv. Appl. Mech.*, **1,** 197–199.

Carr, L. E., III, and R. T. Williams, 1989: Barotropic vortex stability to perturbations from axisymmetry. *J. Atmos. Sci,* **46,** 3177–3191.

Challa, M., and R. L. Pfeffer, 1980: Effects of eddy fluxes of angular momentum on model hurricane development. *J. Atmos. Sci.*, **37,** 1603–1618.

Church, C. R., J. T. Snow, G. L. Baker, and E. M. Agee, 1979: Characteristics of tornado-like vortices as a function of swirl ratio: A laboratory investigation. *J. Atmos. Sci.*, **36,** 1755–1776.

DelSole, T. M., and B. F. Farrell, 1996: The quasilinear equilibration of a thermally maintained, stochastically excited jet in a two-layer model. *J. Atmos. Sci.,* **53,** 1781–1797.

Emanuel, K., 1984: A note on the stability of columnar vortices. *J. Fluid Mech.,* **145,** 235–238.

Farrell, B. F., 1988: Optimal excitation of neutral Rossby waves. *J. Atmos Sci.*, **45,** 163–172.

——, and P. J. Ioannou, 1993: Stochastic forcing of the linearized Navier–Stokes equations. *Phys. Fluids A,* **5,** 2600–2609.

——, and ——, 1994: A theory for the statistical equilibrium energy spectrum and heat flux produced by transient baroclinic waves. *J. Atmos. Sci.*, **51,** 2685–2698.

——, and ——, 1995: Stochastic dynamics of the midlatitude atmospheric jet. *J. Atmos. Sci.,* **52,** 1642–1656.

——, and ——, 1996: Generalized stability theory. Part I: Autonomous operators. *J. Atmos. Sci.,* **53,** 2025–2040.

Fiedler, B. H., 1993: Numerical simulation of axisymmetric tornadogenesis in forced convection. *The Tornado: Its Structure, Dynamics, Prediction, and Hazards,* C. Church, et al., Eds., Amer. Geophys. Union, 41–48.

——, 1994: The thermodynamic speed limit and its violation in axisymmetric numerical simulations of tornado-like vortices. *Atmos.–Ocean*, **32,** 335–359.

——, 1998: Windspeed limits in numerically simulated tornadoes with suction vortices. *Quart. J. Roy. Meteor. Soc.,* **124,** 2377–2392.

Fujita, T. T., 1971: Proposed mechanism of suction spots accompanied by tornadoes. Preprints, *Seventh Conf. on Severe Local Storms,* Kansas City, MO, Amer. Meteor. Soc., 208–213.

Gall, R. L., 1983: A linear analysis of the multiple vortex phenomenon in simulated tornadoes. *J. Atmos. Sci.,* **40,** 2010–2024.

——, 1985: Linear dynamics of the multiple-vortex phenomenon in tornadoes. *J. Atmos. Sci.*, **42,** 761–772.

——, J. Tuttle, and P. Hildebrand, 1998: Small-scale spiral bands observed in Hurricanes Andrew, Hugo, and Erin. *Mon. Wea. Rev.*, **126,** 1749–1766.

Gardiner, C. W., 1985: *Handbook of Stochastic Methods.* 2d ed. Springer-Verlag, 442 pp.

Gent, P. R., and J. C. McWilliams, 1986: The instability of barotropic ciruclar vortices. *Geophys. Astrophys. Fluid Dyn.,* **35,** 209–233.

Guinn, T. A., and W. H. Schubert, 1993: Hurricane spiral bands. *J. Atmos. Sci.,* **50,** 3380–3403.

Ioannou, P. J., 1995: Nonnormality increases variance. *J. Atmos. Sci.*, **52,** 1155–1158.

Kallenbach, R. J., and M. T. Montgomery, 1995: Symmetrization and hurricane motion in an asymmetric balance model Preprints, *21st Conf. on Hurricanes and Tropical Meteorology,* Miami, FL, Amer. Meteor. Soc., 103–105.

Kurihara, Y., 1976: On the development of spiral bands in a tropical cyclone. *J. Atmos. Sci.,* **33,** 940–958.

Leibovich, S., and K. Stewartson, 1983: A sufficient condition for the instability of columnar vortices. *J. Fluid Mech.,* **126,** 335–356.

Lefschetz, S., 1963: *Differential Equations: Geometric Theory.* Dover, 367 pp.

Lewellen, W. S., 1993: Tornado vortex theory. *The Tornado: Its Structure, Dynamics, Predictions, and Hazards,* C. Church et al., Eds., Amer. Geophys. Union, 19–40.

——, D. C. Lewellen, and R. I. Sykes, 1997: Large-eddy simulation of a tornado's interaction with the surface. *J. Atmos. Sci.,* **54,** 581–605.

Loeve, M., 1978: *Probability Theory.* Vol. II, 4th ed. Springer-Verlag, 413 pp.

Melander, M. V., J. C. McWilliams, and N. J. Zabusky, 1987: Axisymmetrization and vorticity-gradient intensification of an isolated two-dimensional vortex through filamentation. *J. Fluid Mech.,* **178,** 137–159.

Michalke, A., and A. Timme, 1967: On the inviscid instability of certain two-dimensional vortex-type flows. *J. Fluid Mech.,* **29,** 647–666.

Montgomery, M. T., and R. J. Kallenbach, 1997: A theory for vortex Rossby waves and its application to spiral bands and intensity changes in hurricanes. *Quart. J. Roy. Meteor. Soc.,* **123,** 435–465.

——, and J. Enaganio, 1998: Tropical cyclogenesis via convectively forced vortex Rossby waves in a three-dimensional quasigeostrophic model. *J. Atmos. Sci.*, **55,** 3176–3207.

Nolan, D. S., 1996: Axisymmetric and asymmetric vortex dynamics in convergent flows. Ph.D. thesis, Harvard University, 279 pp. [Available from University Microfilm, 305 N. Zeeb Rd., Ann Arbor, MI 48106.]

——, and B. F. Farrell, 1999a: Generalized stability analyses of asymmetric disturbances in one- and two-celled vortices maintained by radial inflow. *J. Atmos. Sci.,* **56,** 1282–1307.

——, and ——, 1999b: The structure and dynamics of tornado-like vortices. *J. Atmos. Sci.,* **56,** 2908–2936.

North, G. R., 1984: Empirical orthogonal functions and normal modes. *J. Atmos. Sci.,* **41,** 879–887.

Orr, W. M., 1907: Stability or instability of the steady motions of a perfect liquid. *Proc. Roy. Irish Acad.,* **27,** 9–69.

Pfeffer, R. L., 1958: Concerning the mechanics of hurricanes. *J. Meteor.,* **15,** 113–120.

——, and M. Challa, 1981: A numerical study of the role of eddy fluxes of momentum in the development of Atlantic hurricanes. *J. Atmos. Sci.,* **38,** 2393–2398.

Reasor, P. D., and F. D. Marks, 1999: The asymmetric structure of Hurricane Olivia's inner core. Preprints, *23d Conf. on Hurricanes and Tropical Meteorology,* Vol. I, Dallas, TX, Amer. Meteor. Soc., 301–304.

Rott, N., 1958: On the viscous core of a line vortex. *Z. Agnew Math. Mech.,* **9,** 543–553.

Rotunno, R., 1978: A note on the stability of a cylindrical vortex sheet. *J. Fluid Mech.,* **87,** 761–771.

——, 1984: An investigation of a three-dimensional asymmetric vortex. *J. Atmos. Sci.,* **41,** 283–298.

Smith, G. B., II, and M. T. Montgomery, 1995: Vortex axisymmetrization: Dependence on azimuthal wavenumber or asymmetric radial structure changes. *Quart. J. Roy. Meteor. Soc.,* **121,** 1615–1650.

Smith, R. K., and H. C. Weber, 1993: An extended analytic theory of tropical-cyclone motion in a barotropic shear flow. *Quart. J. Roy. Meteor. Soc.,* **119,** 1149–1166.

Staley, D. O., 1985: Effect of viscosity on inertial instability in a tornado vortex. *J. Atmos. Sci.,* **42,** 293–297.

——, and R. L. Gall, 1979: Barotropic instability in a tornado vortex. *J. Atmos. Sci.,* **36,** 973–981.

——, and ——, 1984: Hydrodynamic instability of small eddies in a tornado vortex. *J. Atmos. Sci.,* **41,** 422–429.

Steffens, J. L., 1988: The effect of vorticity-profile shape on the instability of a two-dimensional vortex. *J. Atmos. Sci.,* **45,** 254–259.

Thompson, W., 1887: Stability of fluid motion: Rectilinear motion of viscous fluid between two parallel planes. *Philos. Mag.*, **24,** 188–196.

Ward, N. B., 1972: The exploration of certain features of tornado dynamics using a laboratory model. *J. Atmos. Sci.,* **29,** 1194–1204.

Whitaker, J. S., and P. D. Sardeshmukh, 1998: A linear theory of extratropical synoptic eddy statistics. *J. Atmos. Sci.,* **55,** 238–258.

Willoughby, H. E., 1992: Linear motion of a shallow-water barotropic vortex as an initial-value problem. *J. Atmos. Sci.,* **49,** 2015–2031.

——, 1994: Nonlinear motion of a shallow water barotropic vortex. *J. Atmos. Sci.,* **51,** 3722–3744.